NASA TN D-760

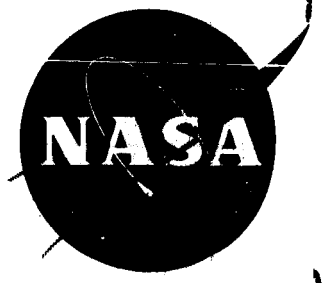

TECHNICAL NOTE

D-760

SKID LANDINGS OF AIRPLANES ON ROCKER-TYPE FUSELAGES

By Wilbur L. Mayo

Langley Research Center
Langley Field, Va.

NATIONAL AERONAUTICS AND SPACE ADMINISTRATION

WASHINGTON

May 1961

NATIONAL AERONAUTICS AND SPACE ADMINISTRATION

TECHNICAL NOTE D-760

SKID LANDINGS OF AIRPLANES ON ROCKER-TYPE FUSELAGES

By Wilbur L. Mayo

SUMMARY

A study is made of the landing of an airplane on a fuselage with "planned" curvature of its lower surface. Initial contact is considered to stop the vertical motion of a point remote from the center of gravity, thus causing rocking on the curved lower surface which converts sinking-speed energy into angular energy in pitch for dissipation by damping forces. Analysis is made of loads and motions for a given fuselage shape, and the contours required to give desired load histories are determined. Most of the calculations involve initial contact at the tail, but there are two cases of unflared landings with initial contact at the nose. The calculations are checked experimentally for the tail-low case.

Even for design sinking speeds the calculated accelerations are frequently less than 1 g; thus skid landings on specially shaped fuselages appear to be quite feasible and merit consideration for special applications. In the calculations for tail-low landings the sinking speed ranges from 3 to 29 ft/sec, the maximum vertical acceleration from 0.25g to 10.4g, the maximum nose-down angular acceleration from 0.25 to 17.1 radians/sec^2, and the maximum nose-up angular acceleration from 0.43 to 21 radians/sec^2. In the nose-low cases a sinking speed of 9 ft/sec gives maximum ground forces 15 and 20 percent of the airplane weight. Experimental check of the calculations and observations on lateral behavior not predicted by the calculations were obtained in tail-low landings of a 1/10-scale dynamic model. In cross winds representing up to 60 mph full scale, the maximum lateral deviation of the model represented about 60 feet full scale.

INTRODUCTION

The first airplane to achieve powered flight made skid landings on its bottom. In the development of aviation there have been recurrent instances of airplanes, after employing special means for take-off, landing on skids. With the development of rocket take-off, vertical risers, and boost-glide vehicles there appeared to be ample reason for reinvestigation of the merits of landing on skids. Such investigation

appeared to be particularly desirable if the lower surface of the airplane could be used so that the skid would not be required to be a special device mounted on a shock-absorbing strut. It has appeared that this might be accomplished, without requiring a deformable landing surface, by suitable sloping of the lower surface of the fuselage so as to convert sinking-speed energy into angular energy in pitch for dissipation largely by aerodynamic damping. The investigation of this possibility forms the basis of the present report. The unexplained statement in reference 1 that the long curved skid is undesirable, and the fact that skid design appears to have been an art rather than a science, added to the challenge of the investigation. Aside from possible application of its results to special-purpose airplanes, it was thought that a contribution might be made to the problems of the wheels-up landing and the hard landing in which collapse of the landing gears is accompanied by impact of the fuselage.

The investigation was hampered by difficulty in assuming undersurface shapes which would give desired load variations, and difficulty in assuming landing conditions and load histories for which reasonable shapes of the fuselage undersurface would be calculated. These difficulties were largely overcome by fixing variables at contact of the center of the fuselage and then employing both forward and backward integration for desired load variations. This procedure had the disadvantage that both the undersurface shape and the landing conditions were results of the calculation, and thus ordinary methods of analysis in which comparisons are made for the same initial conditions or, with other conditions held constant, a single variable is changed, could not be used. Therefore an increased number of calculations and a more complicated analysis of the effects of major variables were necessary. Readers with limited interest in the subject may omit this analysis and may otherwise select data and draw their own conclusions. For this purpose the data summary given in table I, arranged in the same order as the discussion and figures, may be useful. These data are applicable to airplanes which are tail-low at landing speeds. Other data, more limited in scope, may be applied to airplanes which normally land with their fuselage level, if they execute nose-low unflared contacts in order to rock on the curved fuselage undersurface.

SYMBOLS

C_1, C_2, C_3, C_4 coefficients in differential equations, defined by equations (26) to (29)

C_L lift coefficient, $\frac{L}{\frac{\rho}{2} S V^2}$

$C_{L_\alpha} = \frac{\partial C_L}{\partial \alpha}$

C_m aerodynamic pitching-moment coefficient about airplane center of gravity, $2M_a/\rho V^2 S\bar{c}$

$C_{m_\alpha} = \frac{\partial C_m}{\partial \alpha}$

$C_{m_{\dot{\alpha}}} = \frac{\partial C_m}{\partial \left(\frac{\dot{\alpha}\bar{c}}{2V}\right)}$

$C_{m_{\dot{\tau}}} = \frac{\partial C_m}{\partial \left(\frac{\dot{\tau}\bar{c}}{2V}\right)}$

$\bar{c}$ mean aerodynamic chord, ft

D air drag on airplane, lb

E_w energy due to vertical motion of weight not supported by wing lift

F force; ground force normal to the plane of the ground when used without subscript, lb

F_g vertical force applied by external device such as landing gear or arresting gear, lb

g acceleration due to gravity, ft/sec^2

L air lift on airplane, lb

l horizontal distance from contact point to center of gravity, ft

l_t length from rear of fuselage undersurface to center of gravity, measured along reference line of the fuselage, ft

M moment, lb-ft

M_g moment applied by external device such as landing gear or arresting gear, lb-ft

$M_\alpha = \frac{\partial M_a}{\partial \alpha}$

$M_{\dot{\alpha}} = \frac{\partial M_a}{\partial \dot{\alpha}}$

$M_{\dot{\tau}} = \frac{\partial M_a}{\partial \dot{\tau}}$

m	mass of airplane, slugs
n	ratio of F_g to the airplane inertia, $F_g/m\ddot{y}$
R	radius of curvature, ft
R_c	radius of curvature of the rocker at the center position beneath the center of gravity, ft
R_d	radius of evolute circle from which a thread might be unwound to construct the involute rocker on each side of the center of gravity, ft
R_t	radius of curvature of the rocker at the tail point, ft
r	radius of gyration in pitch of airplane, ft
S	wing area, sq ft
T	generalized trim, $\tau\mu$

$\dot{T} = \frac{\partial T}{\partial \theta}$

$\ddot{T} = \frac{\partial \dot{T}}{\partial \theta}$

t	time, sec
V	landing speed, ft/sec
W	weight of airplane, lb
x	distance from center of gravity to point of contact of rocker with ground, measured along reference line of fuselage, positive for rearward contact points, ft (fig. 1)

$\dot{x} = \frac{\partial x}{\partial t}$

Y generalized distance of center of gravity from ground, $y\mu/r$

$\dot{Y} = \frac{\partial Y}{\partial \theta}$

$\ddot{Y} = \frac{\partial \dot{Y}}{\partial \theta}$

y height of center of gravity above ground, ft (fig. 1)

$\dot{y} = \frac{\partial y}{\partial t}$

$\ddot{y} = \frac{\partial \dot{y}}{\partial t}$

z distance from center of gravity to point of contact with ground, measured perpendicular to reference line of fuselage, positive when contact is below reference line, ft (fig. 1)

α angle of attack, relative to angle for zero moment, radians unless otherwise specified

$\dot{\alpha} = \frac{\partial \alpha}{\partial t}$

γ flight-path angle, radians

θ generalized time, $C_1 \frac{Vt}{r}$

μ ratio of ground drag load to ground vertical load (coefficient of friction)

ν ratio of M_g to the angular inertia, $M_g/mr^2\ddot{\tau}$

ρ mass density of air, slugs/cu ft

τ angle between reference line of fuselage and ground, radians unless otherwise specified (fig. 1)

$\dot{\tau} = \frac{\partial \tau}{\partial t}$

$\ddot{\tau} = \frac{\partial \dot{\tau}}{\partial t}$

Subscripts:

a	aerodynamic
b	at first contact with the ground
e	effective or equivalent
f	fuselage reference line
max	maximum
min	minimum
o	the point in time at which the impact of the tail is ended and the action of the rocker is begun

CALCULATIONS

Basis of the Calculations

The calculations were concerned with the determination of loads and motions of an airplane landing and rocking on a curved undersurface such as that shown in figure 1. Most of the cases treated involved tail-low contact where the sequence of motion is of the type depicted in figure 2; here the spilling of wing lift provides an effective force for maintaining contact of the fuselage with the ground during damping of the pitching oscillations that ensue. In two cases the rocking was started by nose-low contact such as that shown in figure 3; here the initial increase of the wing lift requires careful shaping of the lower surface of the fuselage in order to maintain contact during stopping of the center of gravity, and, in fact, spilling of excess wing lift (natural or artificial) may be required to maintain ground contact after the contact point travels its maximum length.

Equations used in the calculations are derived in appendix A. Equations relating initial conditions for these equations to landing conditions prior to impulsive arrest of the point of contact are given in appendix B. In appendix C equations are developed which are approximations to those in appendix A. These approximations were not used in the calculations but were useful in the analysis. The assumptions made in the calculations, for which equations are derived in the appendixes, are:

impulsive arrest of the vertical motion of the effective mass at the point of initial contact, a rigid airframe, a rigid landing surface, constant coefficient of friction due to skidding, and no lag or effect of the ground on air lift or moments. Impulsive stopping of the contact point results in slight decrease of the center-of-gravity velocity before the contact point begins to travel along the length of the fuselage. A special shock absorber may be required to absorb the impulse in actual applications, but its design appears to be largely a matter of engineering and consideration of its details was not necessary in the analysis of subsequent loads and motions.

Results of Calculations

Tail-low landings.- Numerical results of the calculations for tail-low landings are summarized in table I. The data in this table are grouped according to four airplanes, for which the airplane characteristics are given in table II, shapes of the fuselage undersurface are given in figures 4 to 7, and time histories of vertical acceleration, angular acceleration, and trim are given in figures 8 to 11.

Most of the calculations were for a proposed bomber, which in some cases was considered to be equipped with an alternate wing which developed its full lift at higher angles. The second airplane, chosen for the purpose of obtaining an experimental check, was a fighter airplane for which a dynamic model was available. Calculations were made for original and modified lower-surface contours of this airplane. The third configuration was a transport airplane, the double-deck fuselage of which tended to increase the effect of ground friction and decrease vertical accelerations because of increased sweep-up of the rear of the fuselage. The fourth airplane was a research airplane for which the feasibility of fitting simple circular-arc rockers was studied.

In those cases where table I refers to circular arcs or involutes (see fig. 12) these shapes were assumed and the accelerations and motions were calculated. The involutes (figs. 4(a) and 6) were very effective in reducing the high accelerations that occurred near zero trim for the circular-arc rockers (figs. 4(a), 7, 8(a), and 11), but gave high peaks at an intermediate point (figs. 8(a) and 10) and appeared to be desirable only in cases where the center region of the fuselage is weakened by bomb-bay doors.

In those cases where table I refers to the type of load application the accelerations were assumed and the rocker shape calculated. Either the vertical center-of-gravity acceleration or the ground force was assumed to be constant, except that either the angular acceleration or the moment of the ground force about the center of gravity was not

allowed to exceed particular values in most of these calculations (figs. 4(b), 4(c), 5, 8(b), 8(c), and 9).

The landing conditions in table I represent cases in which there is no appreciable delay between stopping of the vertical motion of the effective mass at the tail and the beginning of forward motion of the point of ground contact. Provided the same conditions are maintained at the beginning of this forward motion, the histories of rocking can be interpreted in terms of landing conditions involving higher trims, higher values of wing lift, and either higher or lower sinking speeds, according to the initial value of the wing lift. Such interpretations involve the use of different starting points on histories such as that given in figure 13 for rotation about the tail point. Rotations of this type are calculated from the equations in the appendixes by substituting zero for the local radius of curvature of the rocker contour. Variation of the period of such rotation permits design of the contour for variations of the landing trim.

Nose-low landings.- Airplane characteristics and initial conditions used in the calculations for unflared nose-low landings are given in table III. Calculations were made for the actual contour of the airplane and for the contour required to give a constant force of 15 percent of the weight. In the case of the actual contour, after the ground force dropped to zero at a time when the center of gravity had a sinking speed of 2 ft/sec, retraction of the flaps was assumed to occur in order to maintain contact. Similar spilling of the wing lift would be required in the case of the constant-force contour after the ground-contact point reached the tail. The two contours are shown in figure 14, and their histories of trim, center-of-gravity acceleration, and angular acceleration are given in figures 15 and 16.

EXPERIMENT

Apparatus

Tail-low landings were made with two configurations of a 1/10-scale dynamic model of the fighter airplane considered in the calculations. One configuration had the scale contour of the fighter, with the addition of a 1/4- by 1/4-inch longitudinal strip that protected the undersurface of the model. The other configuration involved the addition of a variable-depth runner to obtain a modified rocker shape that had been calculated to give large reductions of both vertical and angular accelerations. Some tests of this configuration were made with a 1/4- by 1/4-inch rubber strip insert to give some representation of the increased elasticity that might be expected for a full-scale airplane.

The two contours, tested in representation of cases 13 and 14 in table I, are plotted in figure 5 and shown in photographs of the model in figures 17 and 18.

Landings were made by inclining a catapult to the proper flight-path angle and launching the model with the scale velocity. Time histories of normal acceleration, angular acceleration, and ground contact were transmitted to a fixed recorder by wires trailing behind the model. A duplicate run without these wires yielded no noticeable difference in the behavior of the model. The accelerometers had a natural frequency of 100 cycles per second and were damped to 65 percent of critical. The ground-contact record was obtained by landing the model on metal plates placed in a concrete serviceway and using contact of a thin metal strip on the model to complete an electrical circuit. The metal plates were 1/4-inch magnesium, except that after buckles 3/4 inch high were observed on a hot day the plates nearest the catapult were replaced with steel plates 1/2 inch thick.

Experimental Results

Time-history records of center-of-gravity acceleration, angular acceleration, and ground contact are reproduced in figures 19, 20, and 21 for landings of the previously discussed model configurations at a sinking speed of 9 ft/sec. The records for the modified contour were obtained with increased sensitivity of the instrumentation because lower accelerations were expected. Scale factors are indicated on the records and, in order to facilitate comparisons, the corresponding calculated histories and case numbers are also given.

Notation is made on the records to indicate pulses which are due to dropping from the thick plate (full-scale drop of 2.5 inches) and due to joints between the plates. Such pulses cause degeneration of the rocking action into a bouncing action and, in the course of trial-and-error experimentation with the tail spring and its catch for preventing rebound, similar pulses frequently occurred following contact of the spring. The experiments, in general, confirmed the validity of the calculations, the expectation that careful selection of the tail shock absorber would be required, and the idea that irregularities of the landing surface should not be large in comparison with the combined deflections of the model and the landing surface.

The path of the model indicated maximum lateral deviations of 60 feet full scale, even though scaling of estimated cross winds to the full-scale airplane gave values up to 60 mph. In most cases there was a yawing of the model just before stopping, with maximum angles

approaching 90° for the basic configuration and about 45° for the modified configuration. The stopping distance of the model indicated full-scale ground travel in the range of 1,000 to 1,200 feet.

EFFECT OF MAJOR VARIABLES

The analytical determination of the effect of major variables was complicated by the previously mentioned fact that the combination of reasonable shapes and desirable load histories was best achieved by a procedure in which the landing conditions were a result of the calculation and could not be accurately controlled. Because of this complication and the large number of variables involved, the following approximate equations were derived in appendix B in order to focus attention on the major variables:

$$\ddot{y} = \frac{\dot{y}_b^2}{r}\left(\frac{m_e}{m}\right)^2\frac{R}{r}$$

$$\ddot{r} = \frac{\dot{y}_b^2}{r}\left(\frac{m_e}{m}\right)^{3/2}\left(1 - \frac{m_e}{m}\right)^{1/2}\frac{R}{r}$$

These equations were derived by assuming that the conversion of sinking-speed energy into angular energy is the major action in rocking, and that the combined and partly compensating effects of air forces, weight, and skidding friction are negligible. Comments on some of these effects, with indication of conditions for which they become of major importance, are included in the discussions of the effect of $\dot{y}^2/r$, the significance of the scale radius of curvature R/r, and the relation between vertical and angular accelerations (determined by the variation of R/r with m_e/m). In figure 22, the combination of these parameters in the approximate equation for vertical acceleration is compared with previously presented calculated acceleration histories for two sinking speeds. Representation of the major variations can be seen even though the differences due to the combined effects of air forces, weight, and ground friction are large enough to merit consideration.

Effect of $\dot{y}^2/r$

Since the parameter $\dot{y}^2/r$ has the dimensions of acceleration one can expect that accelerations will be proportional to this parameter as shown by the approximate equations, and will be otherwise influenced by

various nondimensional ratios. These ratios may be influenced by $\dot{y}^2/r$ and thereby affect the proportionality indicated by the approximate equation, except that for a given vertical stroke in terms of r the average vertical acceleration must be proportional to $\dot{y}^2/r$. The buildup of angular velocity, the average angular acceleration, and the vertical and angular accelerations for a given point of contact are affected by the ratio of the total energy input to the sinking-speed energy and, according to the differences between these two energies, may deviate from proportionality to $\dot{y}^2/r$.

Proportionality of maximum vertical acceleration to $\dot{y}^2/r$, for a given value of r, is shown in figure 23 for previously presented calculations for sinking speeds of 3, 10, and 17 ft/sec. There is need for caution in assuming the general existence of such proportionality, as may be seen from the study in figure 24 of energy due to vertical motion of weight in excess of the wing lift. The scales in this figure determine an equivalent sinking speed having the same amount of energy. Most of these equivalent sinking speeds are large compared with the design sinking speeds approximated with most of the data, thus indicating the importance of the subject energy relative to the sinking-speed energy. A semiempirical equation for determining this energy is shown in figure 24 to be reasonably accurate.

The great importance of energy due to deviations of the wing lift from the weight is further confirmed by the fact that when this energy subtracted from the sinking speed energy (nose-low impact), the net energy input into rocking, and the associated accelerations, were so low that difficulty was experienced in maintaining ground contact and the angular accelerations due to ground moments were less than those due to air moments (figs. 15 and 16). In both nose-low and tail-low contacts if the sinking speeds are high enough the sinking-speed energy is predominant and the proportionality of acceleration to $\dot{y}^2/r$ indicated by the approximate equation can be used without qualification. The sinking speeds required for this are less in the case where the energies add (tail-low contact), but on the basis of figure 24 they appear to be considerably higher than the design sinking speeds approximated in most of the calculations.

Effect of R/r

The approximate equations previously confirmed in figure 22 indicate that the accelerations are proportional to the ratio R/r. In this ratio the denominator r does not vary in a landing, but serves to establish the scale of the model. The numerator R locates an instantaneous horizontally translating center, directly above the point of contact, about which rotation occurs to give vertical acceleration at the point of contact which is simply the centrifugal acceleration $\dot{\tau}^2 R$ (see eqs. (3) and (43)).

For similar distributions of R and similar variations of $\dot{\tau}$ the maximum accelerations for a given r are proportional to R. In figure 25 previously presented data for circular-arc contours show close agreement with this proportionality. Caution should be used in applying this result, however, since a change of R changes the trim range for a given travel of the contact point and changes energy sources which are affected by trim. Previous study has indicated that large amounts of energy may be involved.

Relation Between $\ddot{\tau}$ and $\ddot{y}$

A minimum value of the maximum angular acceleration for a given buildup of angular energy in a given range of trim requires that $\ddot{\tau}$ be constant. The corresponding vertical acceleration approaches infinity as the moment arm of the ground reaction approaches zero. The condition for a minimum value of the maximum vertical acceleration with a given sinking speed and vertical travel of the center of gravity is a constant $\ddot{y}$. This, however, results in large angular accelerations for large moment arms about the center of gravity. For specified limits on both vertical and angular accelerations the sinking speed that can be tolerated will be a maximum if a period of constant $\ddot{\tau}$ for large moment arms is followed by a period of constant $\ddot{y}$ for small moment arms. Such variations, and approximations thereto based on periods of constant ground moment and constant ground force, are included among the calculations previously presented.

Maximum vertical and angular accelerations resulting from the various calculations for tail-low landings are compared in figure 26 through use of nondimensional acceleration coefficients derived in appendix C. In this plot of angular-acceleration coefficient against vertical-acceleration coefficient the solid slant line represents an approximate upper boundary associated with occurrence of maximum vertical and angular accelerations when the ground force has a maximum arm - for example, at the beginning of a case of constant vertical acceleration. At this time the aerodynamic forces and gravity are normally in approximate equilibrium and equation (38) can be used to show that the slope of the limit line is equal to the maximum value of $(l + \mu y)g/r$ or, with ground friction omitted from the approximate equations, lg/r. This approximation indicates $l/r = 3.3$ for the limit line in figure 26. Actually the line was passed through the highest point, which is for a case of constant vertical acceleration with $l/r = 2.2$. The 50-percent increase of slope from 2.2 to 3.3 occurred primarily because the ground force due to deficiency of the initial wing lift was 50 percent of the ground force associated with acceleration of the center of gravity.

The lower boundary of figure 26 approaches asymptotically a value determined by minimum angular acceleration associated with a constant value of this acceleration (expression (57)). Although this minimum is

reached only when the vertical acceleration is infinity, closeness of some of the data to the minimum facilitated close approximation of the lower boundary.

The left boundary in figure 26 is a curved dashed line fitted to the data and to the lower boundary. The combined boundary represents cases in which reductions in angular accelerations are achieved at the expense of increases in vertical acceleration, and vice versa. Although the minimum value of one of these accelerations can be achieved only at the expense of a large increase in the other, some of the data in the region of the dashed curve indicate that close-to-minimum values of both were achieved. Such cases appear to be optimum for design and, on the basis of data summarized in table I, offer acceptable values of both vertical and angular acceleration at design sinking speeds.

Data for nose-low landings were omitted from figure 26 because there was no pronounced conversion of sinking-speed energy into angular energy, as was assumed in deriving the acceleration coefficients from the approximate equations. These data (figs. 15 and 16) show a reduction of the angular velocity during stopping of the center of gravity after contact at the nose, and thus indicate the removal of energy from the airplane faster than the rate of reduction of sinking-speed energy. This result was caused by increases of wing lift which helped stop the center of gravity, by air moments, and by moments due to ground friction which opposed moments due to vertical ground force. The ability of these effects to absorb large quantities of energy is not surprising; large reductions of energy due to increase of wing lift might be expected in nose-low cases since in the opposite-rotating tail-low case the energy input due to decrease of wing lift beneath the weight was large in comparison with the sinking-speed energy (fig. 24). Of less importance is the fact that energy input due to ground friction in a tail-low case caused a 20-percent increase of the maximum acceleration (fig. 10); reversal of this effect in the nose-low case accounts for an appreciable part of the difference between the two cases.

The energy differences caused angular velocities and accelerations to be much less in nose-low landings than in tail-low landings. The higher sinking speeds that would be permissible would facilitate unflared nose-low contacts of airplanes which ordinarily would contact with their fuselage approximately level after a landing flare. The nose-low method is not feasible for airplanes which normally land at substantial trims, and it has the disadvantage that spilling of the wing lift may be required, as in the previously presented examples, to prevent the increased wing lift from causing loss of contact with the ground. The tail-low method is applicable to airplanes which normally land tail-low, and it has the advantage that decrease of the wing lift permits the weight to become effective in maintaining contact with the ground. Although angular velocities and accelerations are much greater in the

tail-low case, they are acceptable even at sinking speeds typical of present design. These factors explain why the tail-low method has constituted the bulk of the present investigation.

CONCLUSIONS

1. On the basis of analysis and model tests, the method of landing and rocking on a fuselage undersurface of planned curvature to convert sinking-speed energy into angular energy for subsequent dissipation appears promising for special applications.

2. In tail-low landings the accelerations are acceptable and the decrease of the wing lift caused by the rotation permits the weight to exert a powerful stabilizing force in maintaining ground contact and limiting angular rotation.

3. In tail-low landings the energy input due to descent of weight not supported by wing lift may be large in comparison with the sinking-speed energy.

4. In nose-low contacts the increase of wing lift may be a predominant factor in stopping the vertical motion of the center of gravity, thereby greatly reducing angular velocities and accelerations, but spilling of the wing lift may be required in order to prevent rebound.

5. For a rigid fuselage landing on a rigid landing surface, the acceleration of the effective mass at the point of contact with the ground is simply the centrifugal acceleration $\dot{\tau}^2 R$, where $\dot{\tau}$ is the angular velocity and R is the local radius of curvature of the undersurface.

6. In landings at sinking speeds high enough for ground forces to be predominant, minimum angular acceleration is achieved at the expense of large vertical acceleration, and vice versa, but it is possible to shape the undersurface so that close-to-minimum values of both are achieved.

7. The contours required to give acceptable accelerations appear to be reasonable, but contours which otherwise appear to be reasonable will not give acceptable accelerations if there are large fluctuations of radius of curvature over lengths great enough for the fluctuation to integrate to differences in ordinate which are large compared with the local deformation of the fuselage and the landing surface.

8. The experimental data confirmed the expectation that irregularities in the landing surface will be important if they are large in comparison with deformations of the fuselage and landing surface.

9. The experimental data indicated that careful attention must be paid to the mechanism for stopping the vertical motion of the effective mass at the point of first contact so as to establish a smooth transition to rocking on the curved lower surface.

10. The experimental data showed satisfactory directional stability of a dynamic model during landing runout with initial rocking oscillations induced by contact at a sinking speed which would induce limit loads in a landing gear.

Langley Research Center,
National Aeronautics and Space Administration,
Langley Field, Va., January 27, 1960.

APPENDIX A

EQUATIONS USED IN THE CALCULATIONS

Rocker Dynamics

The distance from the center of gravity to the ground plane (see fig. 1) is given by the equation

$$y = x \sin \tau + z \cos \tau \tag{1}$$

Linear and angular velocities are related by the following equation, obtained by differentiating equation (1) and utilizing the geometric relation $dz/dx = \tan \tau$:

$$\frac{\dot{y}}{\dot{\tau}} = x \cos \tau - z \sin \tau \tag{2}$$

where $\dot{y}/\dot{\tau}$ is the distance from the center of gravity to the point of ground contact, measured along the ground.

Linear and angular accelerations are related by the equation

$$\ddot{y} = \dot{\tau}^2 R - \dot{\tau}^2 y + \dot{\tau}\frac{\dot{y}}{\dot{\tau}} \tag{3}$$

obtained by differentiation of equation (2) and use of the geometric relation

$$R = \frac{dx}{d\tau \cos \tau} = \frac{\dot{x}}{\dot{\tau} \cos \tau} \tag{4}$$

Equation (3) corresponds to rotation of the airplane about an instantaneous center located directly above the point of ground contact at a height equal to the radius of curvature R. The first term is the acceleration at the point of contact with the ground, which is simply the centrifugal acceleration about the instantaneous center. The second term corrects for the effect of vertical height in changing vertical components of the centrifugal acceleration about the instantaneous center.

The third term corrects the vertical acceleration of the center of gravity for the effect of angular acceleration about the instantaneous center.

The force and acceleration normal to the plane of the ground are related by the equation

$$F = m\ddot{y} + mg - F_a + F_g \tag{5}$$

The moment due to the vertical ground force on the rocker is

$$M_v = F(x \cos \tau - z \sin \tau) = F\frac{\dot{y}}{\dot{\tau}} \tag{6}$$

and the moment due to ground friction is

$$M_d = \mu y F \tag{7}$$

where

M_v moment due to vertical ground force on the rocker

M_d moment due to drag load at the ground

The angular acceleration is determined from the fact that the angular inertia moment is equal and opposite to the sum of the applied moments. Thus,

$$-mr^2\ddot{\tau} = M_v + M_d + M_a + M_g \tag{8}$$

or, considering equations (6) and (7),

$$-\ddot{\tau} = \frac{F\left(y\mu + \frac{\dot{y}}{\dot{\tau}}\right) + M_a + M_g}{mr^2} \tag{9}$$

Aerodynamic Force and Moment

The vertical aerodynamic force F_a is given by the equation

$$F_a = L \cos \gamma + D \sin \gamma \tag{10}$$

and the aerodynamic moment M_a is given by the equation

$$M_a = M_\alpha \alpha + M_{\dot{\alpha}} \dot{\alpha} + M_{\dot{\tau}} \dot{\tau} \tag{11}$$

Nondimensional Equations

The equations which have been presented are sufficient to permit solution by numerical integration. However, it is expedient to combine and simplify the equations and convert them to a nondimensional basis.

Combining equations (5), (9), (10), and (11) results in the following equation:

$$-\ddot{\tau} = \frac{\left(m\ddot{y} + F_g + W - L \cos \gamma - D \sin \gamma\right)\left(y\mu + \frac{\dot{y}}{\dot{\tau}}\right) + C_{m_\alpha} \alpha S \bar{c} \frac{\rho}{2} V^2 + \left(C_{m_{\dot{\alpha}}} \dot{\alpha} + C_{m_{\dot{\tau}}} \dot{\tau}\right) S \bar{c} \frac{\bar{c}}{2V} \frac{\rho}{2} V^2 + M_g}{mr^2} \tag{12}$$

Equation (12) can be simplified by assuming that (1) $D \sin \gamma$ is negligible compared with $L \cos \gamma$, (2) $\cos \gamma = 1$, (3) $L = C_{L_\alpha} \alpha \frac{\rho}{2} S V^2$ where C_{L_α} is a constant, (4) at first contact with the ground $F_a = W$, (5) moments are in balance at ground contact, (6) the pilot does not move the controls, (7) the flight-path angle γ is represented by the equation $\gamma = \dot{y}/V$, and (8) the velocity V can be considered constant during a landing impact.

With these assumptions,

$$\alpha = \tau - \tau_b - \frac{\dot{y} - \dot{y}_b}{V} + \alpha_b \tag{13}$$

$$\dot{\alpha} = \dot{\tau} - \frac{\ddot{y}}{V} \tag{14}$$

where the subscript b indicates values at the beginning of the landing impact. Equation (12) can then be reduced to the following form in which the terms are arranged so as to be nondimensional:

$$\frac{\ddot{\tau} r}{g} = \left(\frac{-\ddot{y}}{g} + \frac{F_g}{W} + \frac{\tau - \tau_b}{\alpha_b} - \frac{\dot{y} - \dot{y}_b}{\alpha_b V}\right)\left(\frac{y\mu}{r} + \frac{\dot{y}}{r\dot{\tau}}\right) + \frac{\bar{c}\frac{dC_m}{dC_L}}{r}\left[\frac{\tau - \tau_b}{\alpha_b} - \frac{\dot{y} - \dot{y}_b}{\alpha_b V}\right.$$

$$\left. + \left(\frac{\bar{c}C_{m_{\dot{\tau}}}}{2C_{m_\alpha}} + \frac{\bar{c}C_{m_{\dot{\alpha}}}}{2C_{m_\alpha}}\right)\frac{\dot{\tau}}{\alpha_b V} - \frac{\bar{c}C_{m_{\dot{\alpha}}}}{2C_{m_\alpha}}\frac{\ddot{y}}{\alpha_b V^2}\right] + \frac{M_g}{Wr} \tag{15}$$

A nondimensional equation of greater simplicity is obtained by introducing the generalized variables

$$Y = \frac{y\mu}{r} \tag{16}$$

$$T = \tau\mu \tag{17}$$

and differentiating Y and T with respect to the generalized time

$$\theta = C_1 \frac{Vt}{r} \tag{18}$$

to obtain $\dot{Y}$, $\ddot{Y}$, $\dot{T}$, and $\ddot{T}$:

$$\dot{Y} = \frac{\dot{y}\mu}{VC_1} \tag{19}$$

$$\ddot{Y} = \frac{\ddot{y}\mu r}{V^2 {C_1}^2} \tag{20}$$

$$\dot{T} = \frac{\dot{\tau}\mu r}{VC_1} \tag{21}$$

$$\ddot{T} = \frac{\ddot{\tau}\mu r^2}{V^2 C_1^2} \tag{22}$$

Also, it is convenient to introduce the variables n and ν where

$$n = \frac{F_g}{m\ddot{y}} \tag{23}$$

$$\nu = \frac{M_g}{mr^2\ddot{\tau}} \tag{24}$$

With these substitutions, equation (15) reduces to

$$(1 - \nu)\ddot{T} = \left[-\ddot{Y}(1 + n) + T - T_b - C_1\left(\dot{Y} - \dot{Y}_b\right)\right]\left(\dot{Y} + \frac{\dot{Y}}{\dot{T}}\right)$$
$$+ C_2\left[T - T_b - C_1\left(\dot{Y} - \dot{Y}_b\right)\right] + C_3\dot{T} - C_4\ddot{Y} \tag{25}$$

where

$$C_1 = \frac{\rho}{2}\left(\frac{grC_{L_\alpha}}{W/S}\right)^{1/2} \tag{26}$$

$$C_2 = \frac{\bar{c}}{r}\frac{dC_m}{dC_L} \tag{27}$$

$$C_3 = \frac{\left(\frac{\bar{c}}{r}\right)^2\left(C_{m_{\dot{\alpha}}} + C_{m_{\dot{\tau}}}\right)C_1}{2C_{L_\alpha}} \tag{28}$$

$$C_4 = \frac{\left(\frac{\bar{c}}{r}\right)^2 C_{m_{\dot{\alpha}}} C_1^2}{2C_{L_\alpha}} \tag{29}$$

In obtaining the equation of motion (15) and the simplified equation (25), use was made of an equation for the applied force (eq. (5)). The first term in parentheses in equation (15) represents $-F/W$; that is,

$$\frac{F}{W} = \frac{\ddot{y}}{g} - \frac{\bar{F}g}{W} - \frac{\tau - \tau_b}{\alpha_b} + \frac{\dot{y} - \dot{y}_b}{\alpha_b V} \tag{30}$$

The first bracketed term in the simplified equation (25) represents $-\frac{F}{W}\mu\alpha_b$; that is,

$$\frac{F}{W}\mu\alpha_b = \ddot{Y}(1 + n) - T + T_b + C_1\left(\dot{Y} - \dot{Y}_b\right) \tag{31}$$

The motions and inertia loads resulting from the unknown rockers which give a particular history of $\frac{F}{W}\mu\alpha_b$ may be determined through use of equations (25) and (31) and a numerical integration procedure. Assumed values of the force must correspond to an upward push on the airplane since the ground is incapable of exerting a downward pull.

The complete history of the motions and inertia loads of the unknown rockers which give a particular history of either $\ddot{Y}$ or $\ddot{T}$ can be obtained from equation (25) without use of equation (31). However, when the accelerations are small or do not obviously correspond to an upward push of the ground on the airplane, equation (31) should be used as a check to see that the impossible condition of downward pull of the ground on the airplane is not implied by the assumed acceleration history.

After determining the motion history of the unknown rockers which gives a desired load application, the unknown shapes may be obtained from the following equations, which come from equations (1) and (2):

$$\frac{x}{r} = \frac{Y}{\mu}\sin\frac{T}{\mu} + \frac{\dot{Y}}{\dot{T}}\cos\frac{T}{\mu} \tag{32}$$

$$\frac{z}{r} = \frac{Y}{\mu}\cos\frac{T}{\mu} - \frac{\dot{Y}}{\dot{T}}\sin\frac{T}{\mu} \tag{33}$$

When loads and motions are to be determined for a rocker of known shape, the generalized vertical-acceleration parameter $\ddot{Y}$ is determined by the generalized form of equation (3):

$$\ddot{Y} = \dot{T}^2\frac{R - y}{\mu r} + \ddot{T}\frac{\dot{Y}}{\dot{T}} \tag{34}$$

This equation is used in combination with equation (25) to obtain the complete loads and motions of a rocker of known contour. The radius R and the center-of-gravity height y may be explicit functions associated with a mathematical rocker or may be determined by numerical means for a rocker of arbitrary shape. The ability of the rocker to maintain continuous ground contact is determined by use of equation (31) to check on the sign of the computed force. In designs with small trim change during arrest of the tail, an approximate assumption of the force-time curve applied by the shock absorber will be sufficiently accurate for determining τ_o.

When a value of τ_o is determined a check should be made to insure that it is as large as the trim at which the rocker begins its working stroke. If this condition is not met the rocker will impact on a point closer to the center of gravity and receive a shock load. To allow for some variation in landing the rocker should be designed so that τ_o normally is greater than the trim at which the rocker cam becomes effective. This introduces in the early part of the rocking a period of rotation about the end point of the rocker to which the equations for the cam-shaped rocker are applicable through the consideration of the radius of curvature at the point of ground contact as zero.

The initial height of the center of gravity y_o may be determined from equation (1) by substituting the initial trim and the coordinates of the end point. This presupposes that the shock absorber is vertically positioned on the airplane so that the end point of the rocker contacts the ground at the completion of the arrest of this point. In order for a given shock absorber to fulfill this condition over a wide range of sinking speeds it should be of a constant-stroke type in which the applied forces are proportional to the square of the sinking speed. This force characteristic may be obtained from the vertically alined telescoping shock strut in which fluid is squeezed through an orifice at a rate proportional to the telescoping velocity. Such a shock strut also has the advantage that forces tending to extend the strut after arrest of the end point may be sufficiently small to prevent rebound and subsequent impact at another point on the rocker. This is particularly important when the trim after arrest of the tail is greater than the trim at which the rocker begins its working stroke, with the result that there is a period of rocking in which only aerodynamic moments due to motion set up by arrest of the tail are available for holding the tail on the ground.

APPENDIX B

INITIAL CONDITIONS

The initial conditions to be used in the equations of appendix A are those which exist after the vertical motion of the tail has been stopped by the tail shock absorber. These conditions (indicated by the subscript o) are related to those at the beginning of tail impact (indicated by the subscript b) by momentum considerations related to the impulse required to stop the vertical velocity of the tail at contact with the ground. This impulse is equal to $m_e\dot{y}_t$, where m_e is the effective mass at the tail. The change in vertical momentum of the center of gravity is also equal to this impulse, so that

$$m\left(\dot{y}_b - y_o\right) = m_e\dot{y}_{t,b} \tag{35}$$

or

$$\dot{y}_o = \dot{y}_b - \frac{m_e}{m}\dot{y}_{t,b} \tag{36}$$

where $\dot{y}_{t,b}$ may be obtained from the equation

$$\dot{y}_t = \dot{y} - \dot{\tau}l$$

Here l is the horizontal distance from contact point to center of gravity and m_e/m is determined as follows.

The inertia of the effective mass at the tail and the center of gravity are both equal to the ground force and are equal to each other. Thus,

$$m_e\ddot{y}_t = m\ddot{y} \tag{37}$$

where

$$\ddot{y}_t = \ddot{y} - \ddot{\tau}l$$

The angular acceleration is related to the vertical acceleration by the condition that the sum of the angular-inertia moment, the vertical-force moment, and the ground friction moment is equal to zero. Thus

$$\ddot{\tau}\left(mr^2\right) + F(l + \mu y) = 0$$

or

$$\ddot{\tau}\left(mr^2\right) + m\ddot{y}(l + \mu y) = 0$$

Then

$$\ddot{\tau} = -\frac{\ddot{y}(l + \mu y)}{r^2} \tag{38}$$

From equation (37),

$$\frac{m_e}{m} = \frac{1}{1 - \frac{\ddot{\tau}}{\ddot{y}} l}$$

Substituting equation (38) gives

$$\frac{m_e}{m} = \frac{1}{1 + \left(\frac{l + \mu y}{r^2}\right) l} \tag{39}$$

or, when μ during the tail impulse is equal to μ during the subsequent rocking,

$$\frac{m_e}{m} = \frac{1}{1 + \left(\frac{\dot{Y}}{\dot{T}}\right)^2 + \left(\frac{\dot{Y}}{\dot{T}}\right) Y} \tag{40}$$

The trim τ_o is given by the equation

$$\tau_o = \tau_b + \dot{\tau}_b t_i + \int\int^{t_i} \ddot{\tau}\, dt\, dt \tag{41}$$

where the duration of the tail impulse t_i and the integral are determined by the design of the tail shock absorber.

APPENDIX C

APPROXIMATE VARIATION OF VERTICAL AND ANGULAR ACCELERATIONS

The variation of the vertical and angular accelerations can be approximated by assuming that the gain in angular energy is equal to the loss of sinking-speed energy (negligible or compensating effects of unbalanced weight, skidding friction, and air moment). Such an assumption is most reasonable for design impacts which involve maximum sinking-speed energy and maximum accelerations, and hence are of the greatest interest. With the above assumption,

$$mr^2\dot{\tau}^2 = m\dot{y}_b^2 - m\dot{y}^2$$

and, with $\dot{y} = \dot{\tau}l$,

$$mr^2\dot{\tau}^2 = m_e\dot{y}_b^2 \tag{42}$$

where (see eq. (39))

$$m_e = \frac{m}{1 + \frac{l^2}{r^2}}$$

The vertical acceleration at any instant may be determined on the basis that the instantaneous center of rotation is directly above the point of ground contact at a distance equal to the radius of curvature of the rocker at this point (eq. (3)). Thus the vertical acceleration of the effective mass is simply the centrifugal acceleration due to this radius - the term $\dot{\tau}^2R$ of equation (3). The acceleration at the center of gravity is related to the acceleration of the effective mass through the fact that both inertia forces are equal since they are both equal to the vertical force. Therefore

$$m\ddot{y} = m_e\dot{\tau}^2R \tag{43}$$

Combining equations (42) and (43) gives

$$\ddot{y} = \frac{\dot{y}_b^2}{r^2}\left(\frac{m_e}{m}\right)^2 R \qquad (44)$$

The angular acceleration is determined by the relation that the angular inertia is equal to the applied torque. This may be expressed as follows, where the inertia of the effective mass has been substituted for the ground force:

$$mr^2\ddot{\tau} = m_e\dot{\tau}^2 R l \qquad (45)$$

Combining equations (43), (44), and (45) yields the following equation for angular acceleration:

$$\ddot{\tau} = \frac{\dot{y}_b^2}{r^3}\left(\frac{m_e}{m}\right)^{3/2}\left(1 - \frac{m_e}{m}\right)^{1/2} R \qquad (46)$$

These approximate equations permit the calculation of acceleration histories without the necessity of performing the numerical integrations required by the more exact equations used in the present investigation. They show that for a given point of contact the radius of curvature of the lower surface contour at that point is the sole geometric parameter affecting the accelerations, and that accelerations are proportional to this radius of curvature. Decrease of the radius of curvature may be used to reduce the associated ground forces to any desired value, but excessive use of this means will result in angles of the contour slope greater than the landing trim and thereby cause contact to occur at a point which is closer to the center of gravity. This increases the effective mass at the point of initial contact, and the increased shock of initial contact tends to offset the subsequent reduction in force. To reduce the shock of initial contact to a minimum and insure contact at the same point over a reasonable range of landing trims so that a special shock absorber can be effective, it will be generally desirable to limit the integrated effect of curvature so that

$$\left(\frac{dz}{dx}\right)_{max} < \tau_{min}$$

For a given strength distribution of the airplane, the optimum lower surface contour will generally be that for which the curvature integrates to the indicated maximum and is so distributed that the critical sinking speed causes a critical load to occur at some point at all times. In comparing results for different curvature distributions, corrections should be made for the effects of integration to different maximum slopes. With a view toward this purpose let

$$\frac{R}{r} = \frac{R_c}{r} f\left(\frac{x}{r}\right) \tag{47}$$

where

R_c characteristic radius of curvature

$f\left(\frac{x}{r}\right)$ function describing the curvature distribution

Equation (4) can be reduced to

$$R = \frac{dx}{d\tau} \tag{48}$$

on the basis that the range of $\cos \tau$ is very close to unity. Combining equations (47) and (48) yields

$$d\tau = \frac{r}{R_c} \frac{d\left(\frac{x}{r}\right)}{f\left(\frac{x}{r}\right)} \tag{49}$$

from which it is apparent that

$$\tau \propto \frac{r}{R_c} \tag{50}$$

Combining this with equations (44) and (46) and considering that, for a particular curvature distribution, R at a particular x/r is proportional to R_c, gives

$$\ddot{y}_\tau \propto \frac{\dot{y}_b^2}{r} \tag{51}$$

$$\ddot{\tau}_{r\tau} \propto \frac{\dot{y}_b^2}{r} \tag{52}$$

The proportionality of acceleration to $\dot{y}_b^2$ indicated in equation (52) stems from equation (42) which assumes that the angular energy is equal to the loss of sinking-speed energy. Since a semiempirical expression for energy due to unbalanced weight has been presented (fig. 24), use of it to modify expressions (51) and (52) appears desirable. From equation (42),

$$\frac{1}{2}mr^2\dot{\tau}_{max}^2 = \frac{1}{2}m\dot{y}_b^2 \tag{53}$$

and it is desirable now to use the equation

$$\frac{1}{2}mr^2\dot{\tau}_{max}^2 = \frac{1}{2}m\dot{y}_b^2 + E_w \tag{54}$$

The desired change will be effected if $\dot{y}_b^2$ in equation (53) is replaced by $\dot{y}_b^2 + 2g\frac{E_w}{W}$. Using the equation for E_w from figure 24 and rearranging expressions (51) and (52) to isolate constants of proportionality results in the following acceleration coefficients representing these constants:

$$\frac{\ddot{y}_{max} r_\tau}{\dot{y}_b^2 + 2g\left(1 - 0.7\frac{L_o}{W} - 0.3\frac{L_{y_{min}}}{W}\right)\left(y_o - y_{min}\right)} \tag{55}$$

$$\frac{\ddot{\tau}_{max} r^2_\tau}{\dot{y}_b^2 + 2g\left(1 - 0.7\frac{L_o}{W} - 0.3\frac{L_{y_{min}}}{W}\right)\left(y_o - y_{min}\right)} \tag{56}$$

These acceleration coefficients are plotted against each other in figure 26, which presents the results of various calculations that were made.

Through use of equation (54) the angular-acceleration coefficient (56) can be written

$$\frac{\ddot{\tau}_{max}\tau}{\dot{\tau}^2_{max}} \tag{57}$$

From this form of the angular-acceleration coefficient one can determine that its minimum value occurs for constant angular acceleration and is equal to 1/2. Thus

$$\frac{\ddot{\tau}_{max} r^2 \tau}{\dot{y}_b^2 + 2g\left(1 - 0.7\frac{L_o}{W} - 0.3\frac{L y_{min}}{W}\right)\left(y_o - y_{min}\right)} \geqq \frac{1}{2} \tag{58}$$

(within the limits of the various assumptions that have been made) defines the lower boundary in figure 26 if τ is converted to degrees as in this figure.

REFERENCE

1. Barnaby, Ralph Stanton: Gliders and Gliding. The Ronald Press Co., c.1930.

TABLE I

SUMMARY OF CALCULATIONS FOR TAIL-LOW LANDINGS

Case	Sinking speed, $\dot{y}_b$, ft/sec	Initial trim,[a] τ_b, deg	Initial L_b/W	Coefficient of friction, μ	Rocker type	Maximum vertical acceleration, $\ddot{y}/g$	Maximum angular acceleration, $\ddot{\tau}$, radians/sec^2	Maximum negative trim, τ, deg
					Bomber airplane			
1	3	7	1	0.4	Involute	0.25	-0.25, 0.43	3.5
2	10	7	1	.4	Involute	1.37	-.98, 1.27	5.8
3	17	7	1	.4	Involute	4.00	-2.4, 3.3	8.0
4	17	8.6	1	.4	Circular arc	5.6	-2.3	----
5	9.2	5.6	1	.4	Limited moment[b]	.9	-2.0	----
6	19.8	16.5	.9	.4	Limited moment[b]	1.5	-1.65	----
7	17.7	12.5	.8	.4	Limited moment[b]	3.0	-1.8	----
8	25.8	19.6	1	.4	Limited moment[b]	6.0	-2.83	----
9	10.1	6.2	1	.4	Constant acceleration	.9	-3.6	----
10	13.2	9.7	.6	.4	Constant acceleration	.9	-3.2	----
11	13.1	14.2	.7	.4	Constant acceleration	.67	-3.3	----
12	29.0	7	.7	.4	Constant acceleration	6.0	-17.1	----
					Fighter airplane			
13	9	13	1	0.4	Unmodified[c]	10.4	-16, 21	10.7
14	9.6	12.5	1	.4	Limited moment[c,d,e]	2.5	-6.7, 12	
15	9.6	12.5	1	.4	Limited moment[c]	2.5	-6.7, 6.7	----
16	9.6	12.5	1	.4	Limited moment[d,f]	2.5	-6.7, 24.6	----
17	9.4	11.4	.9	.4	Limited moment[g]	3.3	-6.7	----
					Transport airplane			
18	10	13	1	0.4	Involute, R_c = 0 ft	1.0	-1.07	----
19	10	13.5	1	.4	Involute, R_c = 33 ft	1.13	-1.0, 1.52	9
20	10	14.5	1	.4	Involute, R_c = 120 ft	1.35	-1.0	----
21	10	14.5	1	0	Involute, R_c = 120 ft	1.0	-.77	----
					Research airplane			
22	10	11.8	1	0	Circular arc, 88-ft radius	8.1	-15.6	----
23	10	17.2	1	0	Circular arc, 57-ft radius	5.6	-10.9, 11.4	13

[a]Based on 1° change in trim between tail contact and start of forward movement of contact point.

[b]Moment of the vertical ground force limited to that produced by W/2 applied at the tail.

[c]Checked by experiment.

[d]F = 3W when $\ddot{\tau}$ is less than indicated value.

[e]Flaps assumed to be raised at zero trim.

[f]Forebody computed without limitation of moment.

[g]F = 4W when $\ddot{\tau}$ is less than indicated value.

TABLE II

AIRPLANE CHARACTERISTICS USED IN COMPUTATIONS

FOR TAIL-LOW LANDINGS

	Bomber	Fighter	Transport	Research
W/S, lb/sq ft	74	46	78	(a)
V, knots	112	100	112	(a)
C_{L_α}	5.1, [b]3.2	4.2	4.1	[4]C_L, [c]3C_L
α_f for L = W, deg	9, [b]25	16	16	14, [c]19
l_t, ft	55	18.6	70	16.9
r, ft	25	6.6	22	5.9
$\bar{c}$, ft	11	8.09	21	(a)
C_{m_α}	-0.4	-0.3	-0.4	(a)
$C_{m_{\dot{\tau}}}$	[d]-40	-7.14	[d]-18	(a)
$C_{m_{\dot{\alpha}}}$	(e)	-2.86	(e)	(a)

[a]This characteristic was removed from consideration by assuming C_{L_α} to have the indicated relation to the C_L at landing, by assuming changes in γ to be small compared with changes in τ, and by omitting changes in aerodynamic moment.

[b]Alternate wing.

[c]Alternate wing or lower landing speed.

[d]$C_{m_{\dot{\tau}}} \frac{\bar{c}^2}{4 l_t^2} = 0.4$.

[e]Assumed to be of negligible importance.

TABLE III

AIRPLANE CHARACTERISTICS USED IN CALCULATIONS

FOR NOSE-LOW LANDING

[Raising of flaps assumed to have negligible effect on trimming moments, or to have its effect canceled by control movement.]

W, lb	58,750
V, knots	140
$\dot{y}$, ft/sec	9
S, sq ft	1,175
$\bar{c}$, ft	16.8
r, ft	10.9
C_{L_α}	4.5
$\frac{\partial C_m}{\partial C_L}$	-0.13
C_{m_α}	-0.58
$C_{m_{\dot{\alpha}}}$	-2.9
$C_{m_{\dot{\tau}}}$	-7.1

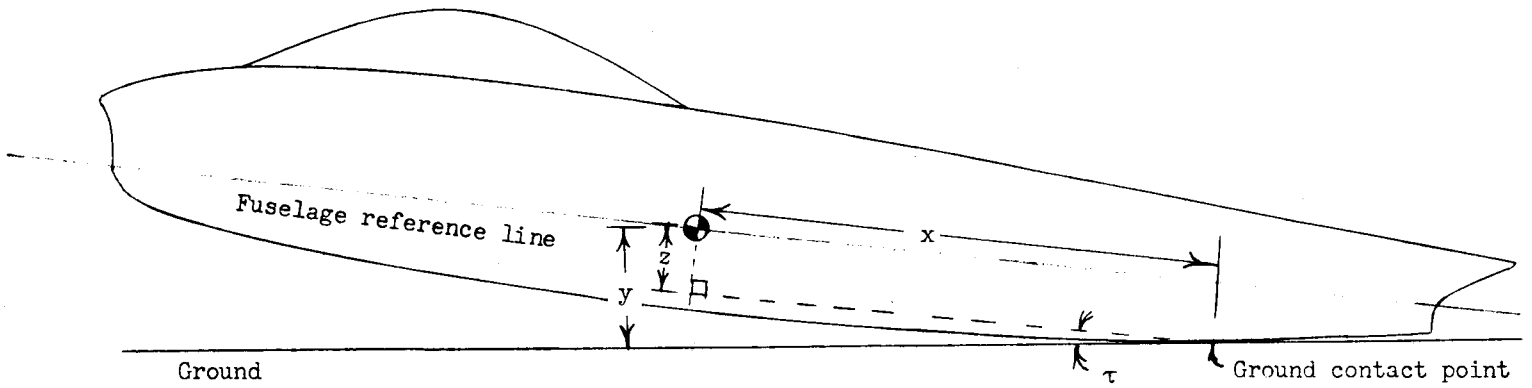

Figure 1.- Geometry of a rocker landing.

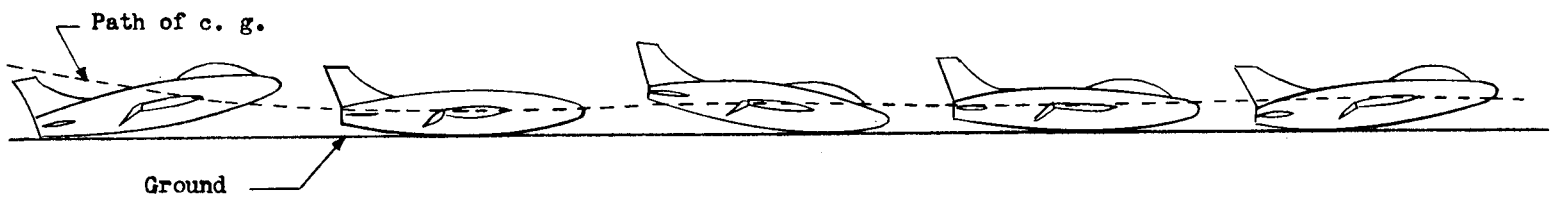

Figure 2.- Motion sequence in a tail-low rocker landing.

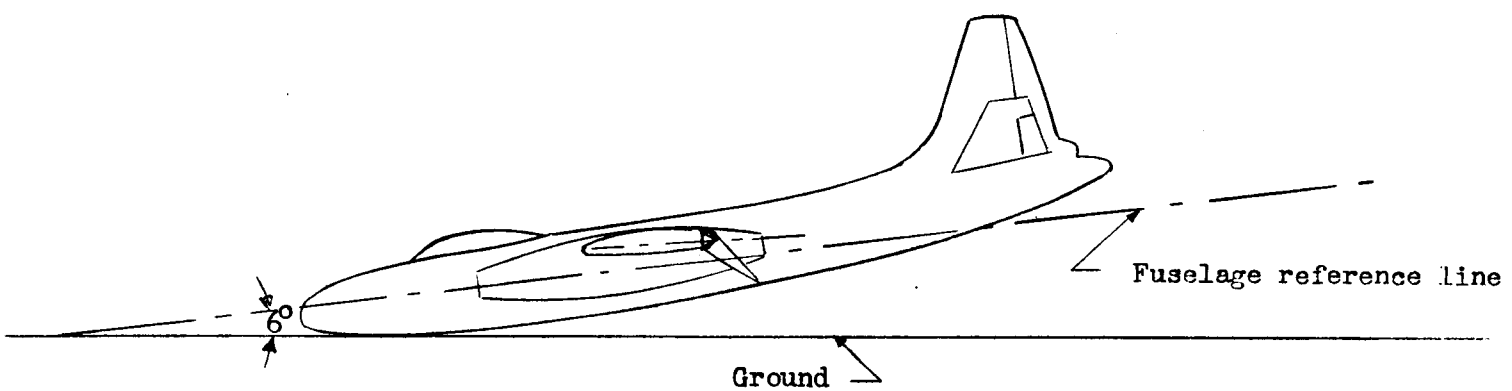

Figure 3.- Airplane at nose contact after compression of shock absorber.

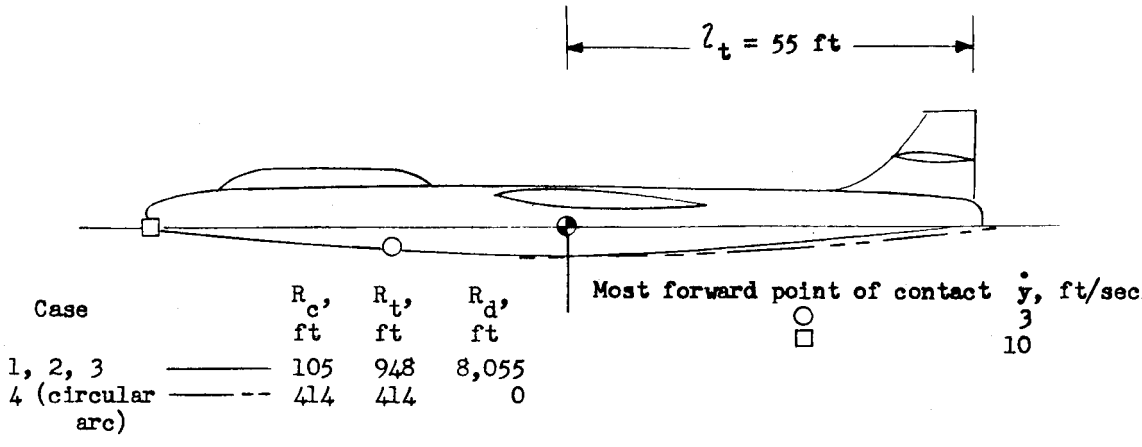

(a) Involute.

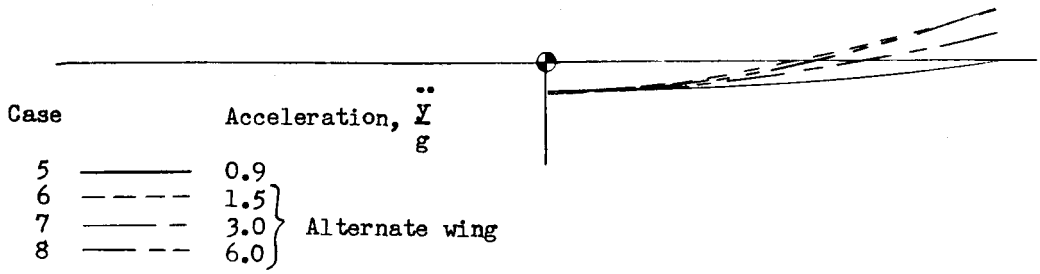

(b) Limited moment.

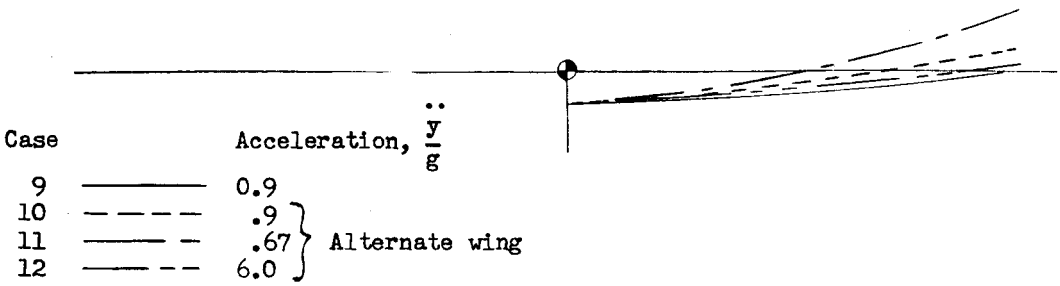

(c) Constant acceleration.

Figure 4.- Rockers for bomber airplane.

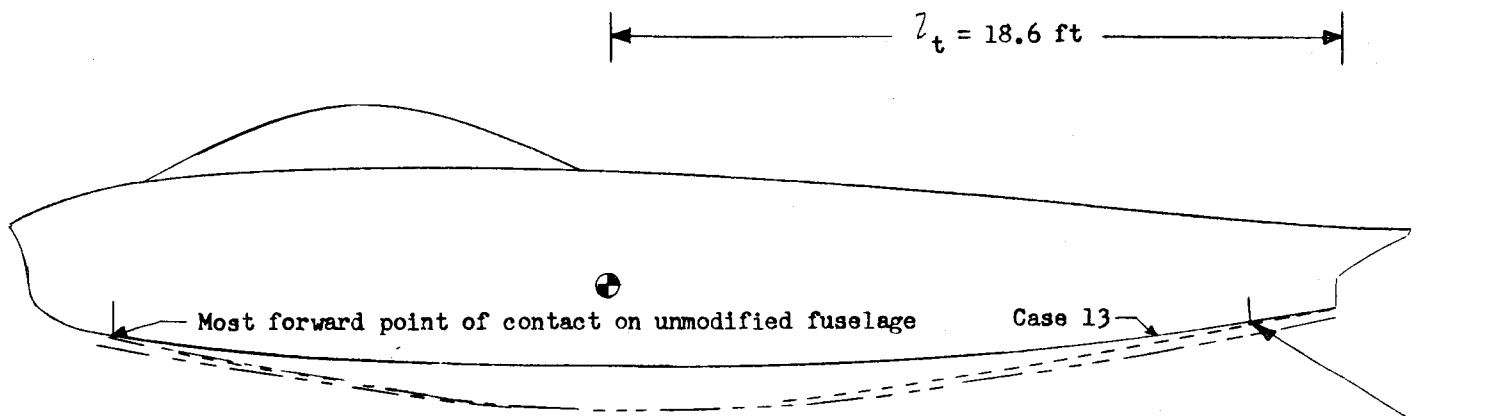

Case		$\frac{F}{W}$	$\ddot{\tau}$, radians/sec^2
Afterbody	Forebody		
14,15,16	15 — — — —	≤ 3	≤ 6.7
	14 ——— –	≤ 3	≤ 12.0
	16 ——— – –	$= 3$	Unlimited
17	——— – – –	≤ 4	≤ 6.7

Figure 5.- Rockers for fighter airplane.

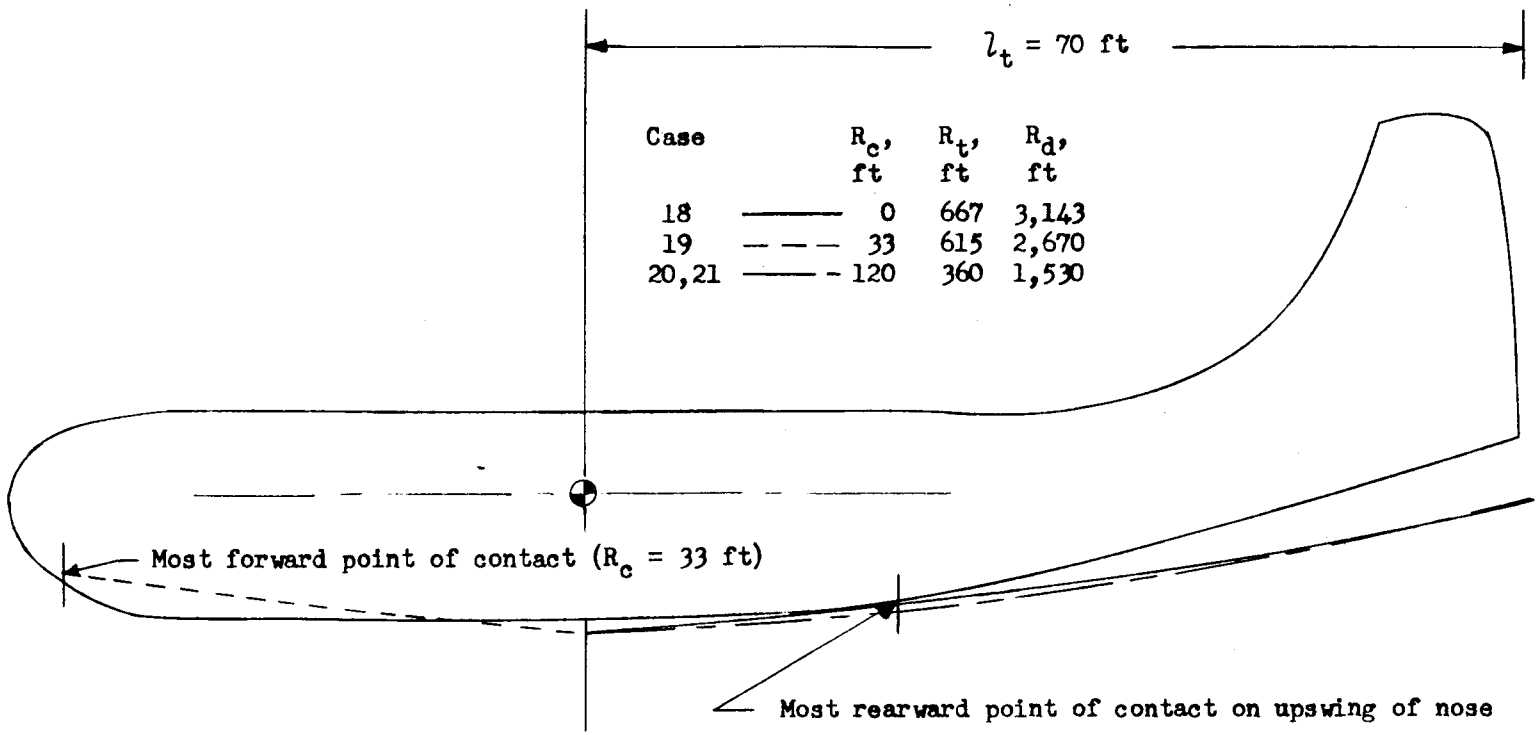

Figure 6.- Rockers for transport airplane.

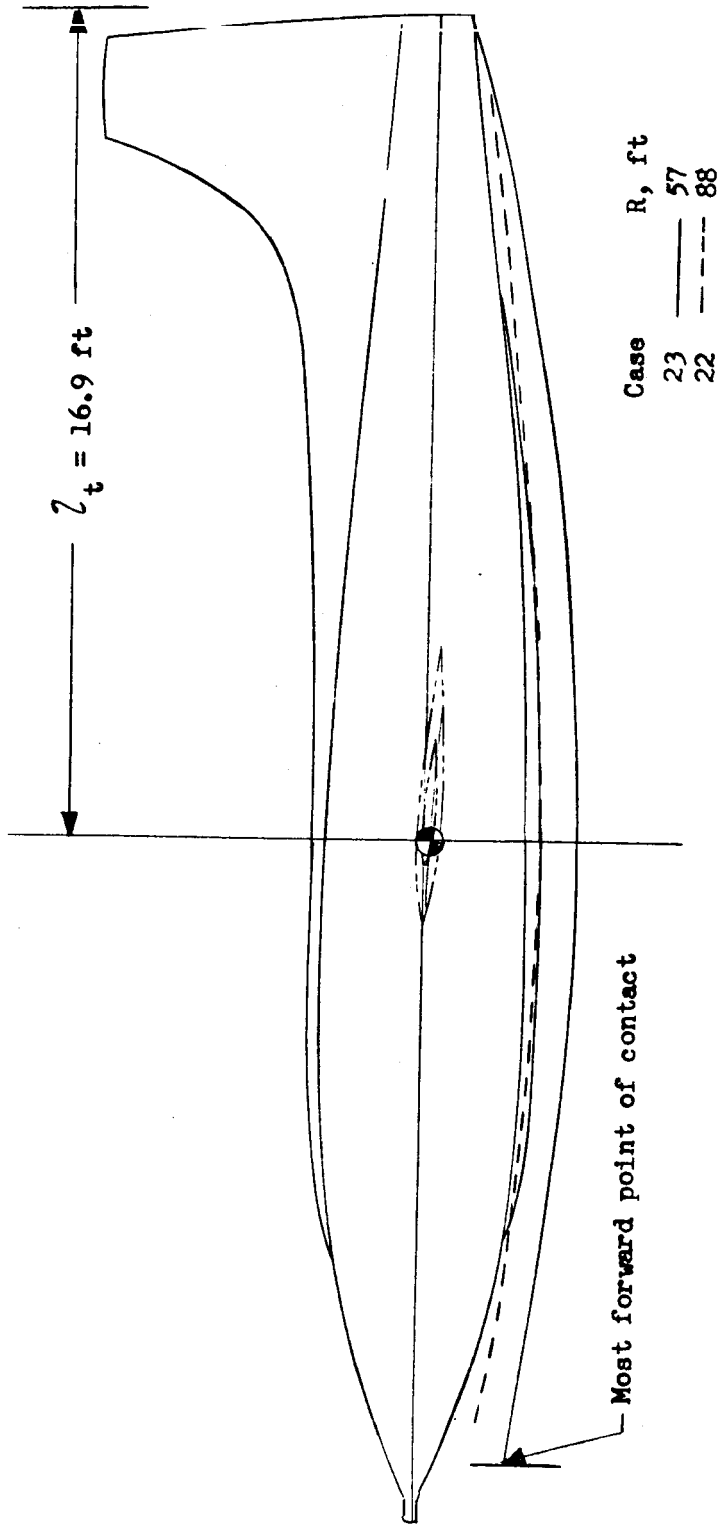

Figure 7.- Rockers for research airplane.

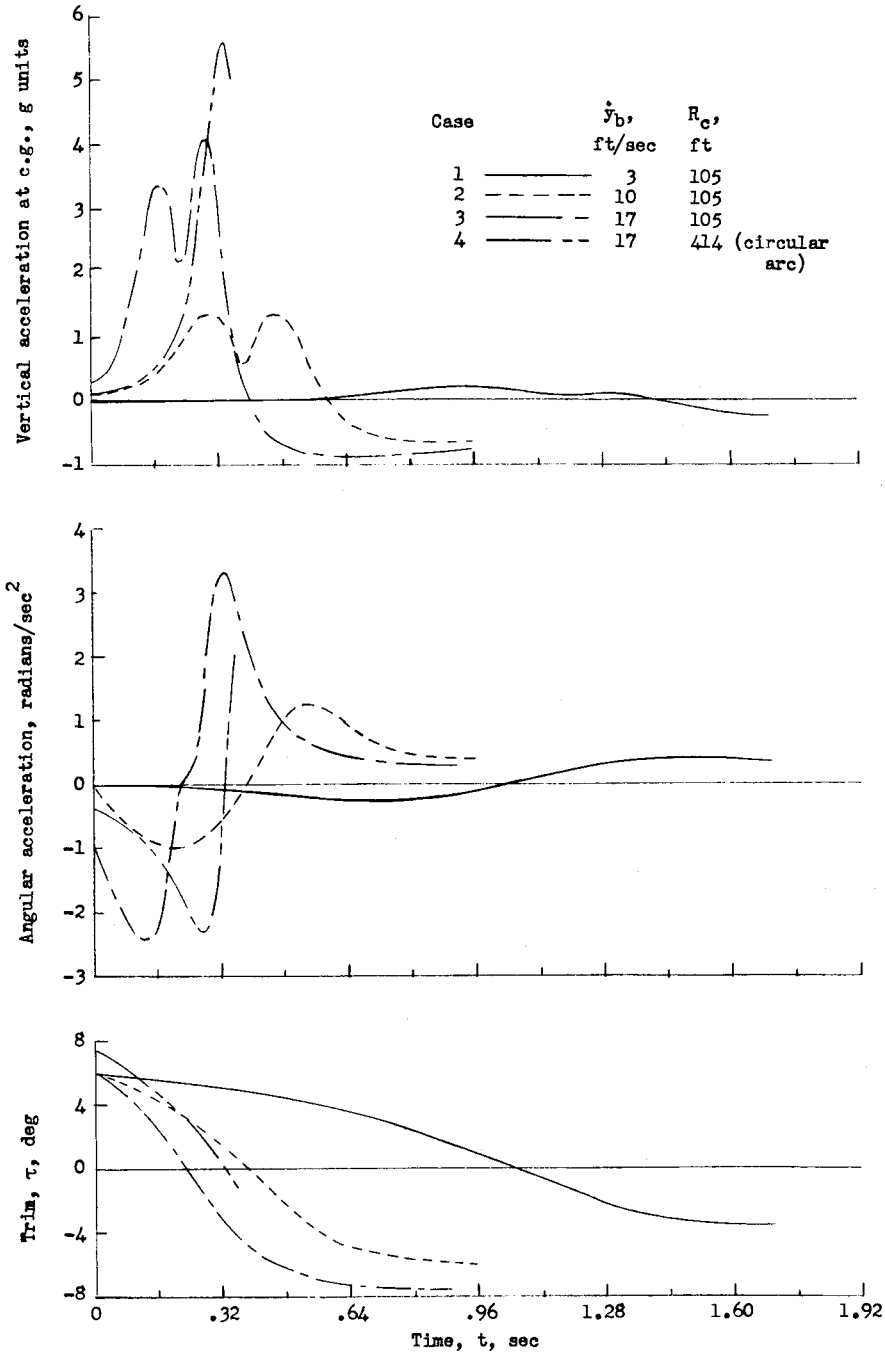

(a) Involute.

Figure 8.- Time histories of vertical acceleration, angular acceleration, and trim for bomber. $\mu = 0.4$.

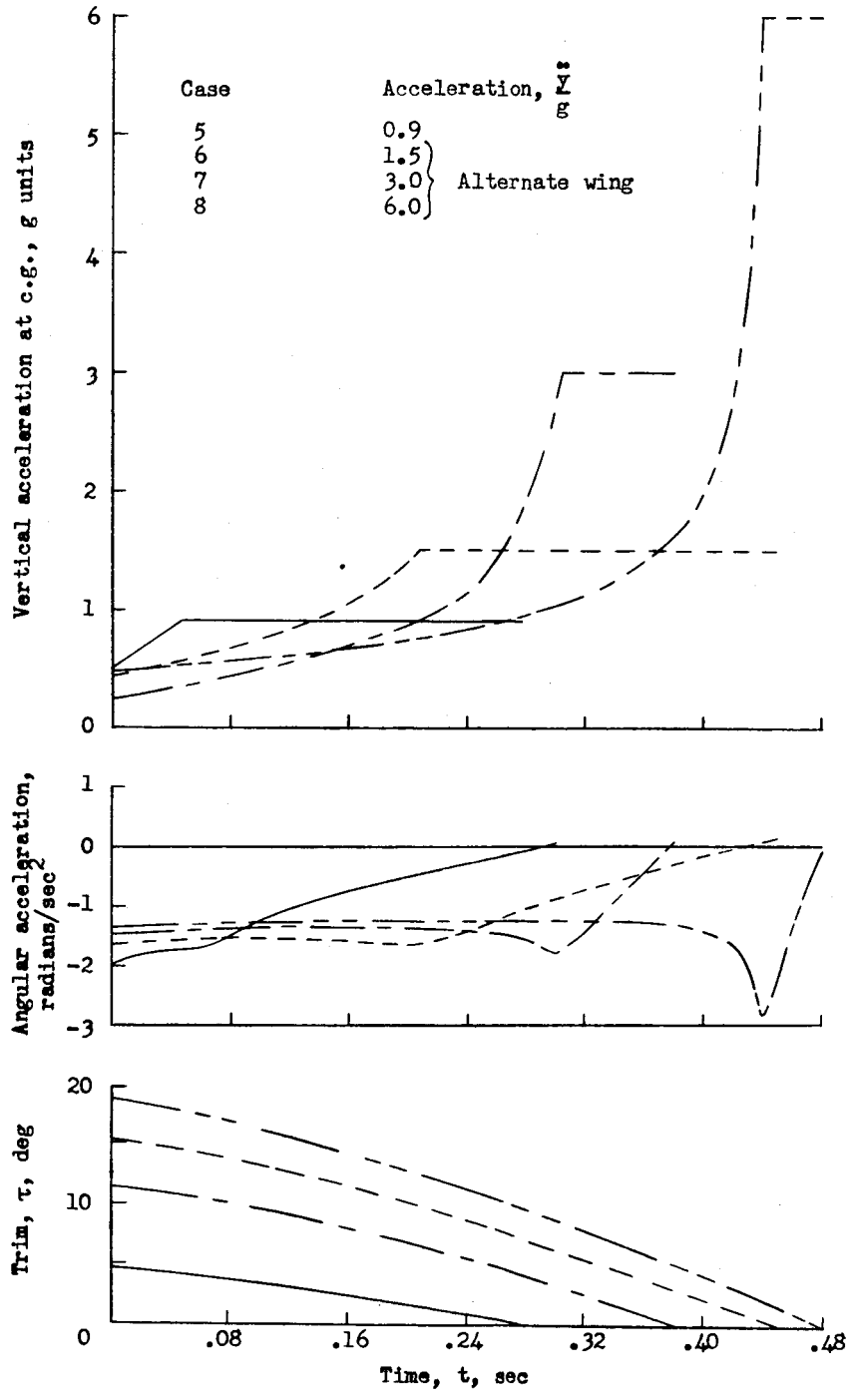

(b) Limited moment.

Figure 8.- Continued.

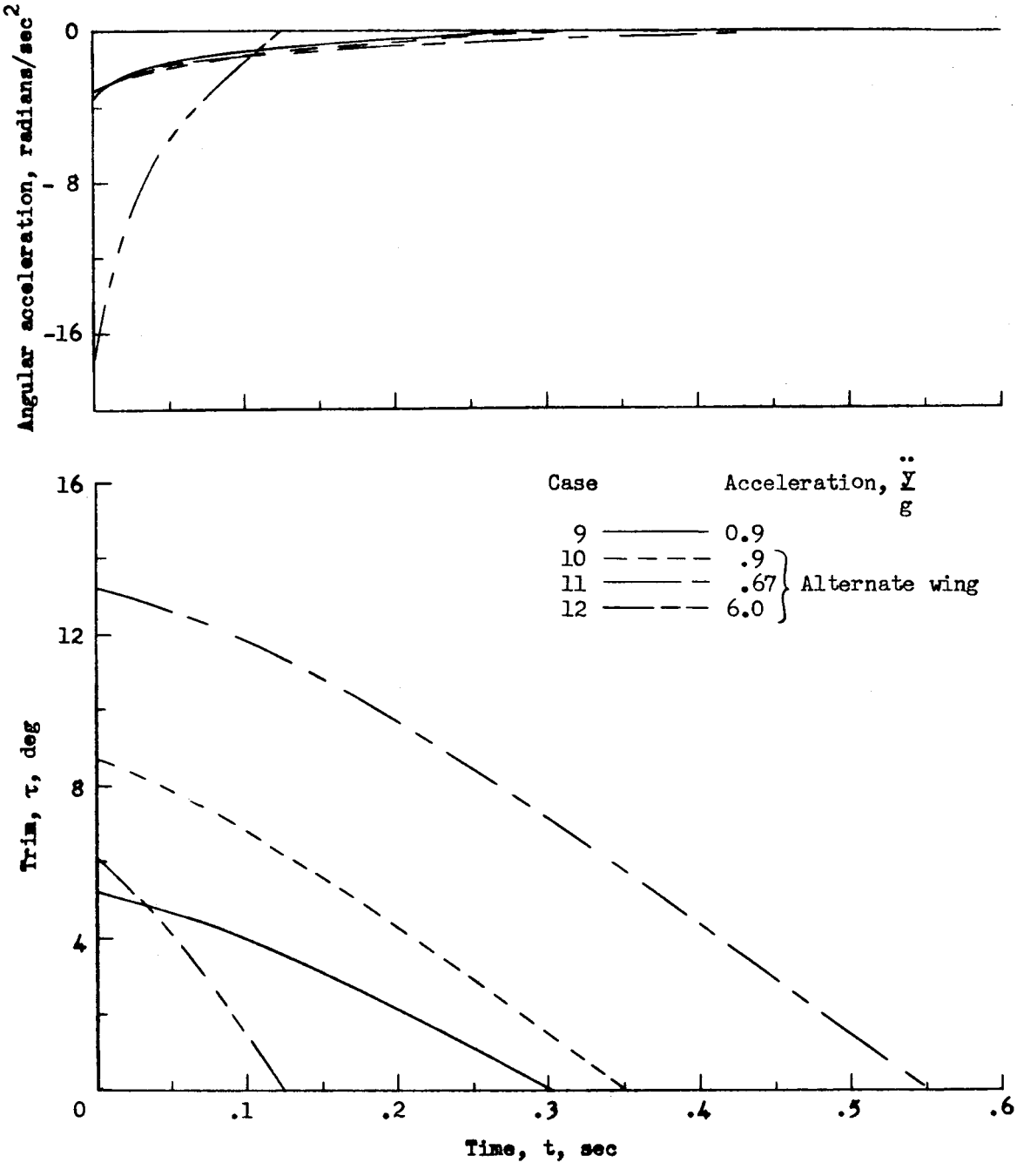

(c) Constant acceleration.

Figure 8.- Concluded.

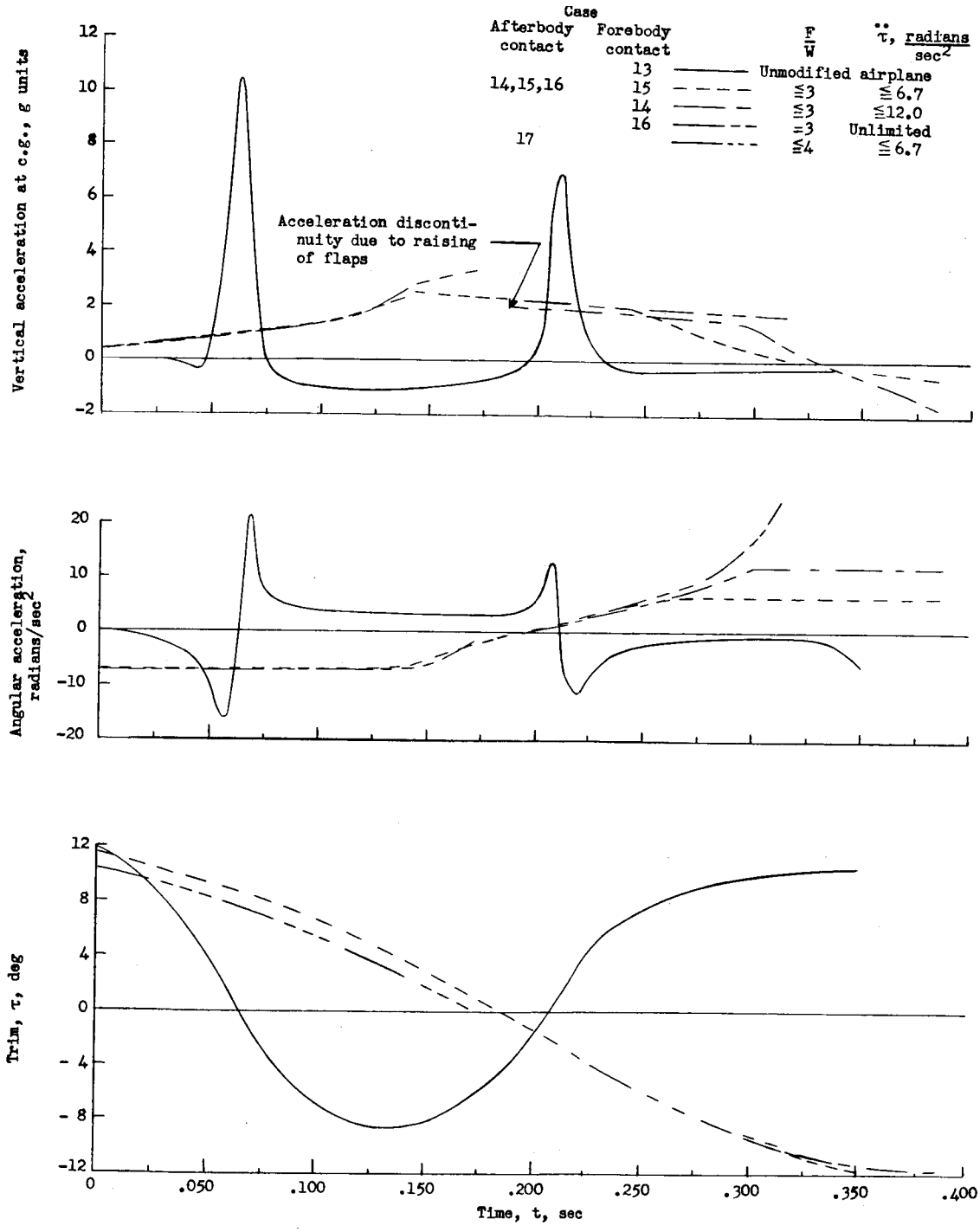

Figure 9.- Time histories of vertical acceleration, angular acceleration, and trim for fighter.

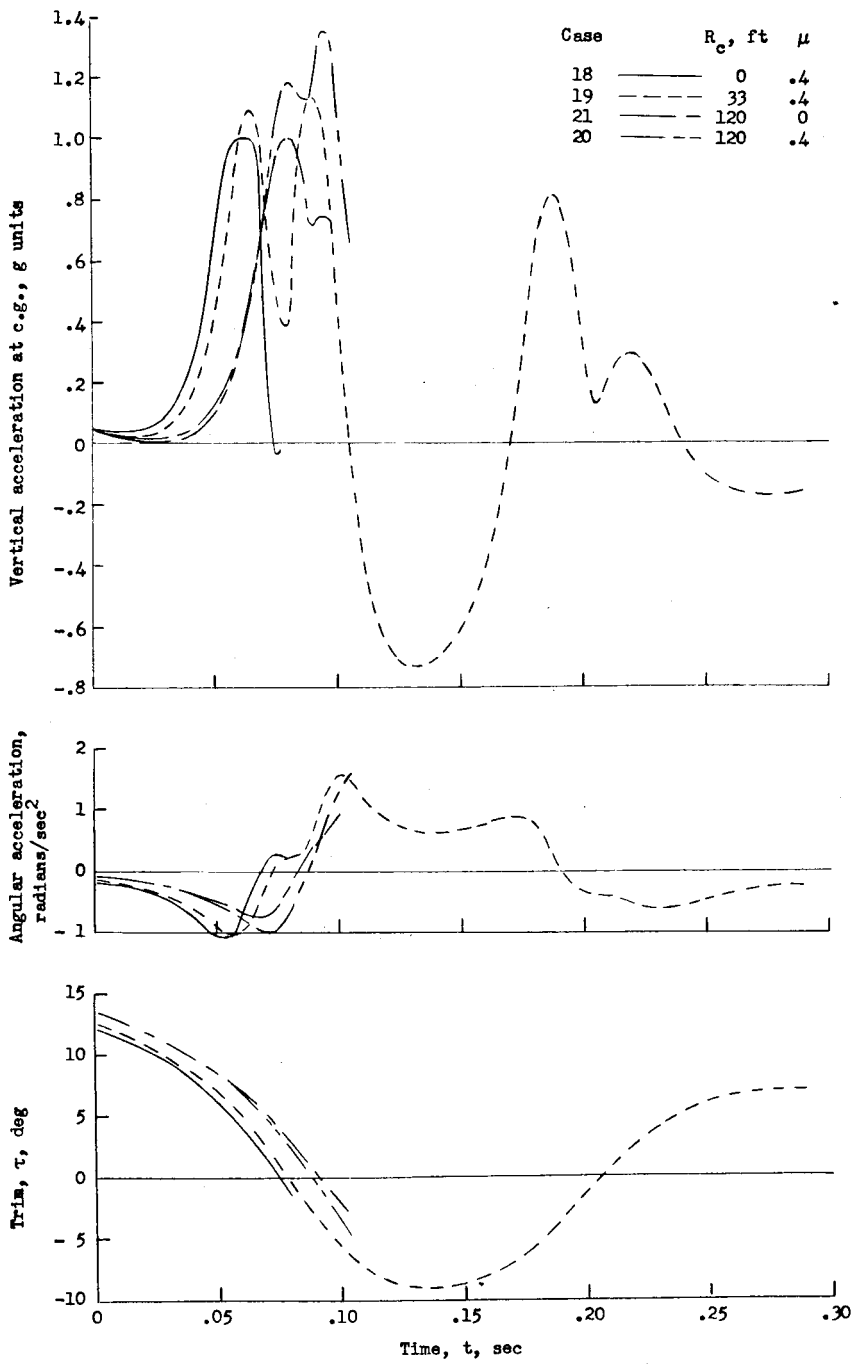

Figure 10.- Time histories of vertical acceleration, angular acceleration, and trim for transport airplane with a sinking speed of 10 feet per second.

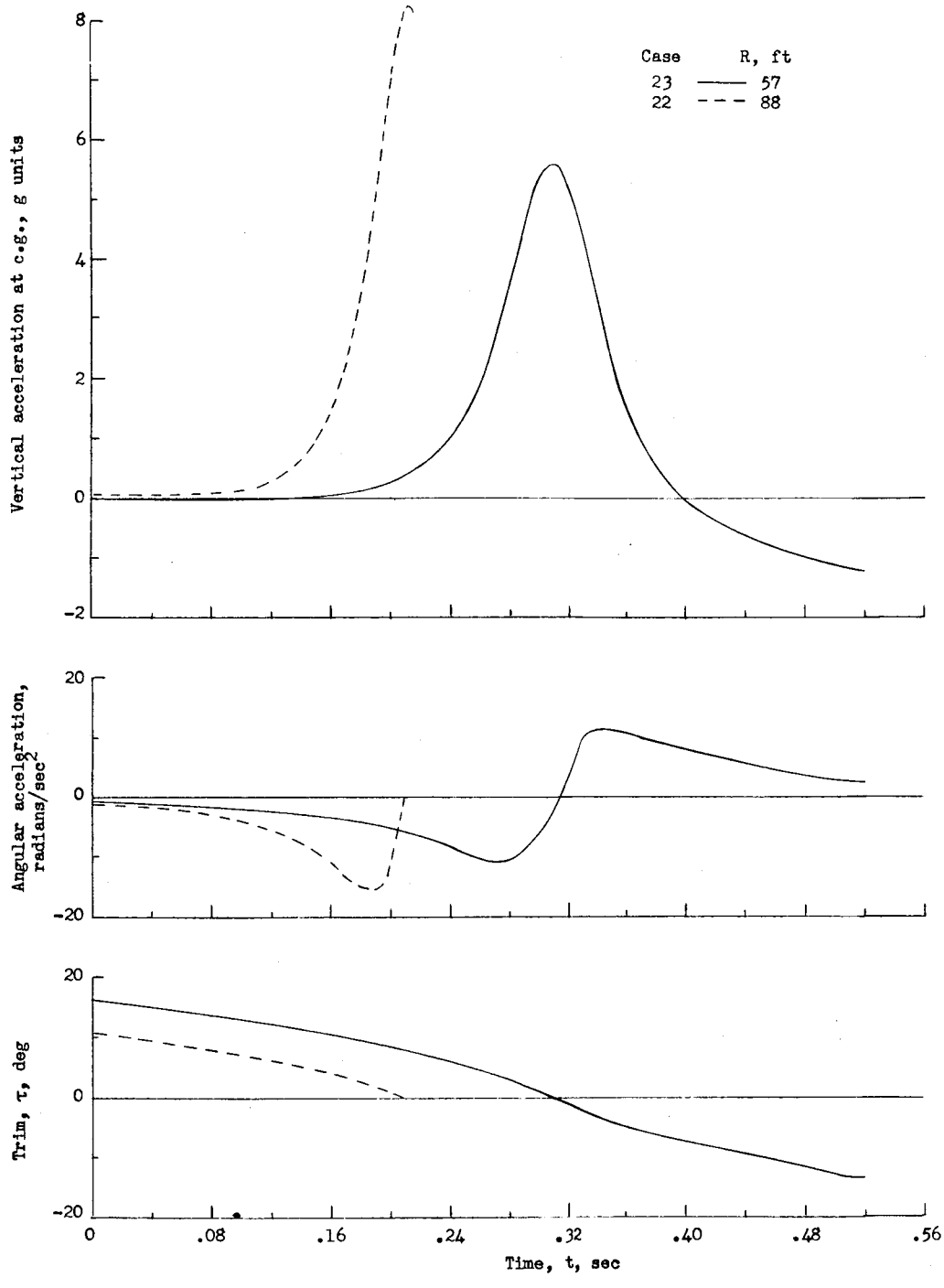

Figure 11.- Time histories of vertical acceleration, angular acceleration, and trim for research airplane with a sinking speed of 10 feet per second.

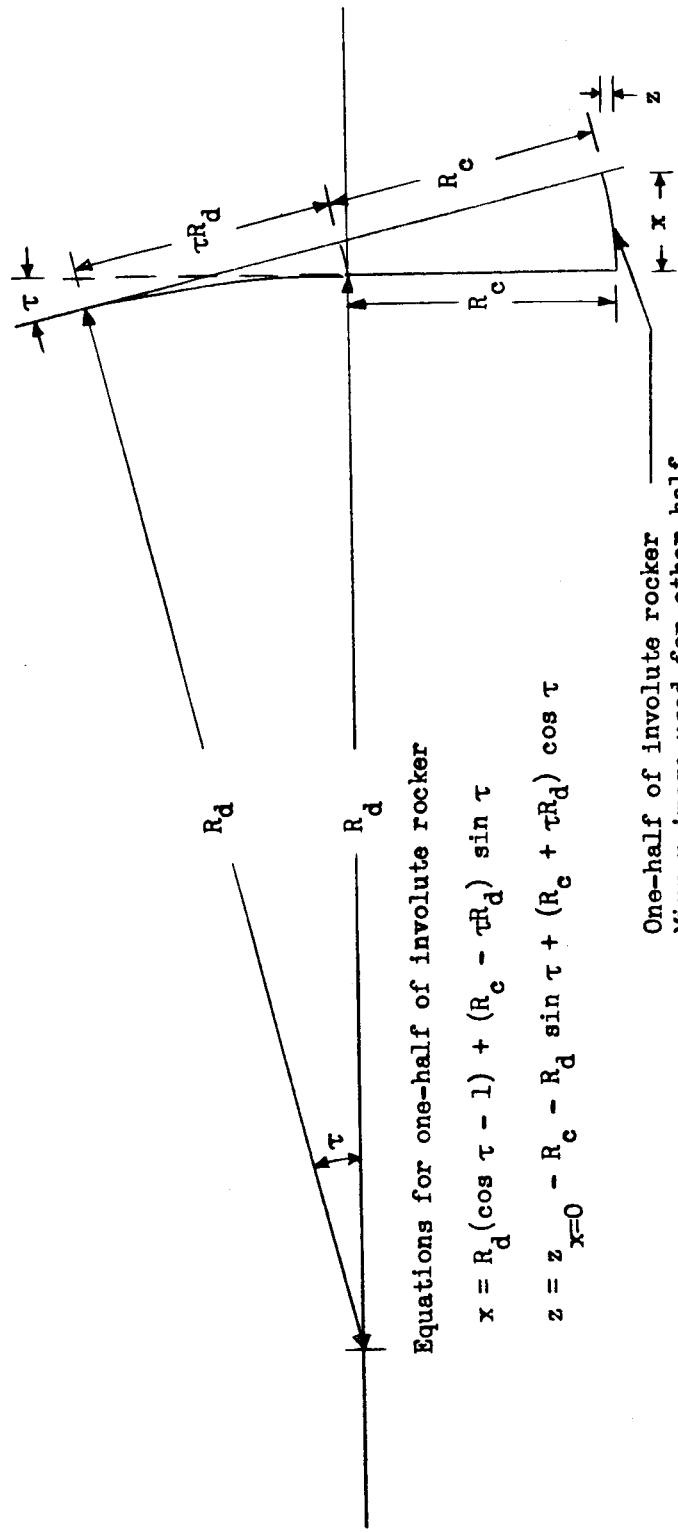

Figure 12.- Geometry of involute rockers used in calculations.

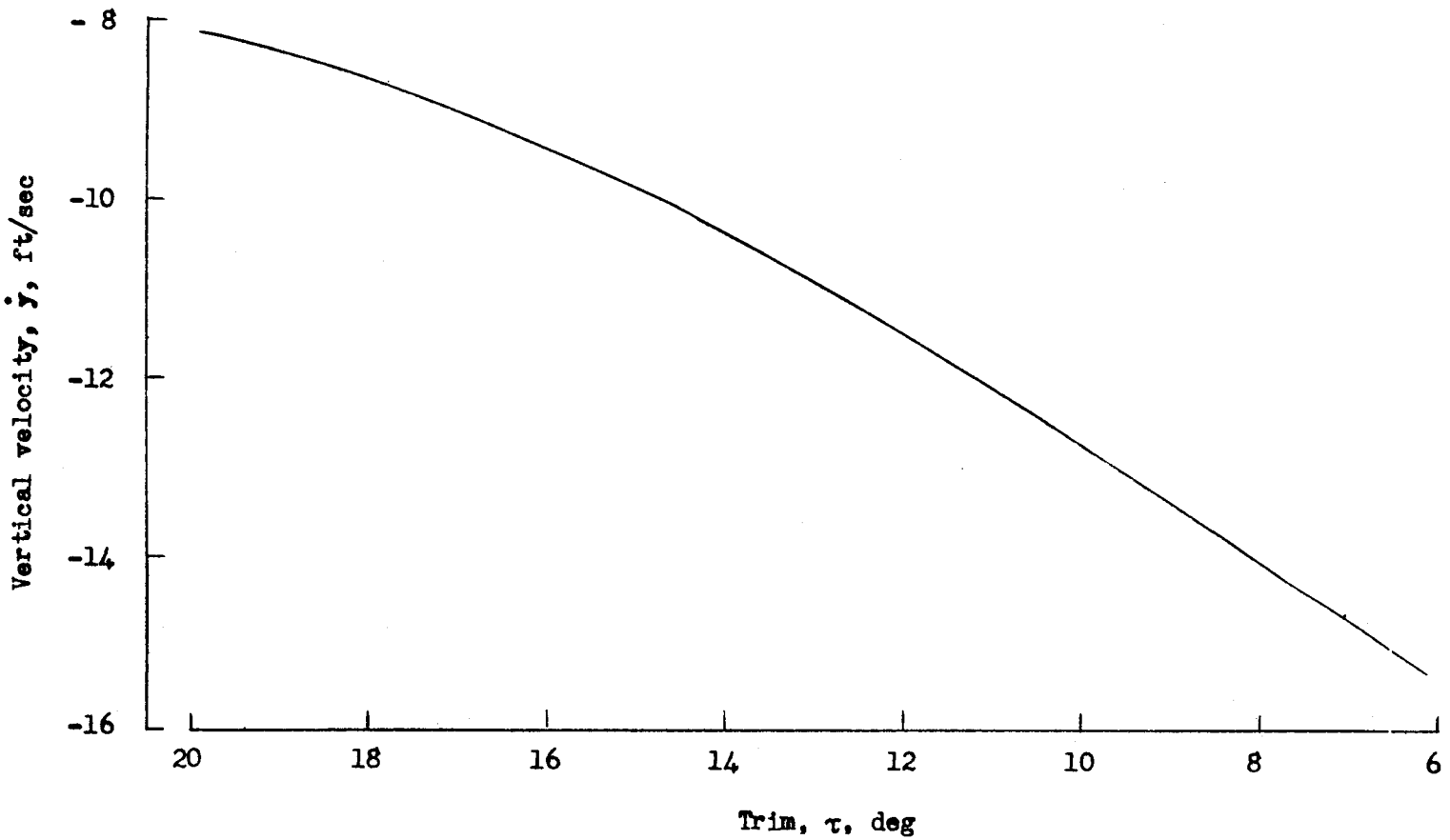

Figure 13.- Variation of vertical velocity of center of gravity with trim during rotation about tail point. Bomber alternate wing; initial wing lift, 1 g; vertical velocity, 10 feet per second prior to tail impact.

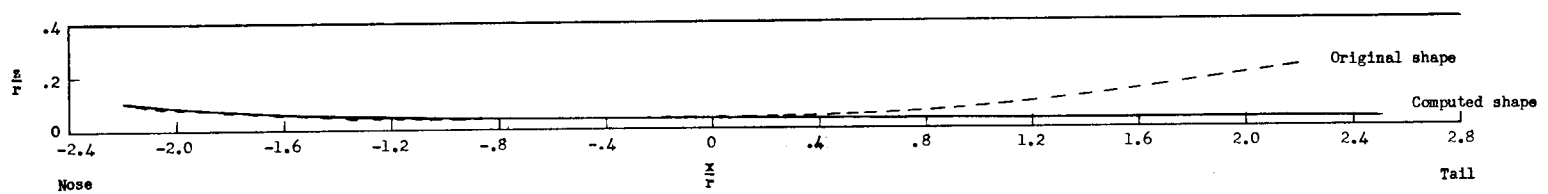

Figure 14.- Lower surface contours for nose-low landings.

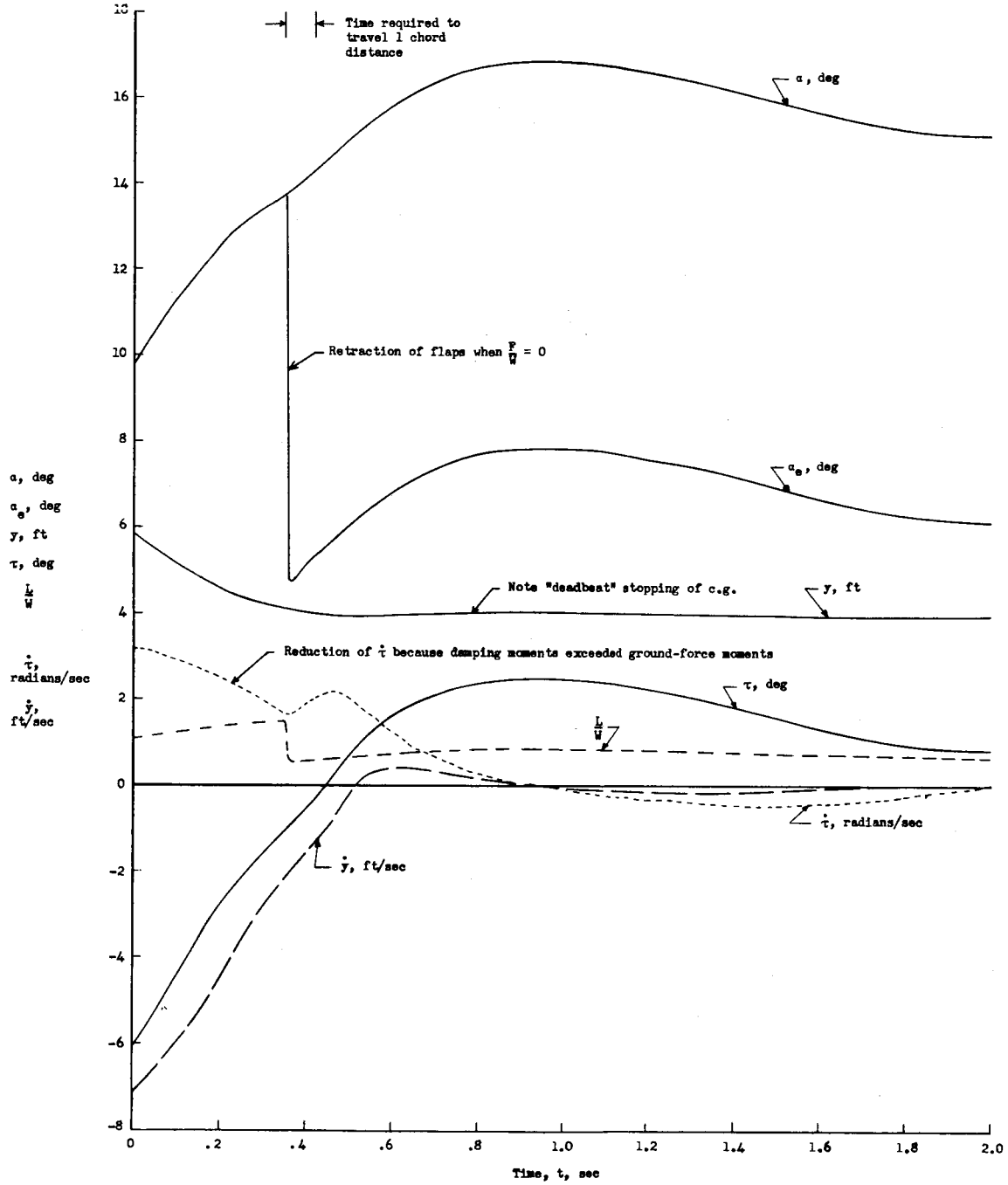

Figure 15.- Load and motion histories for nose-low landing. Unmodified contour.

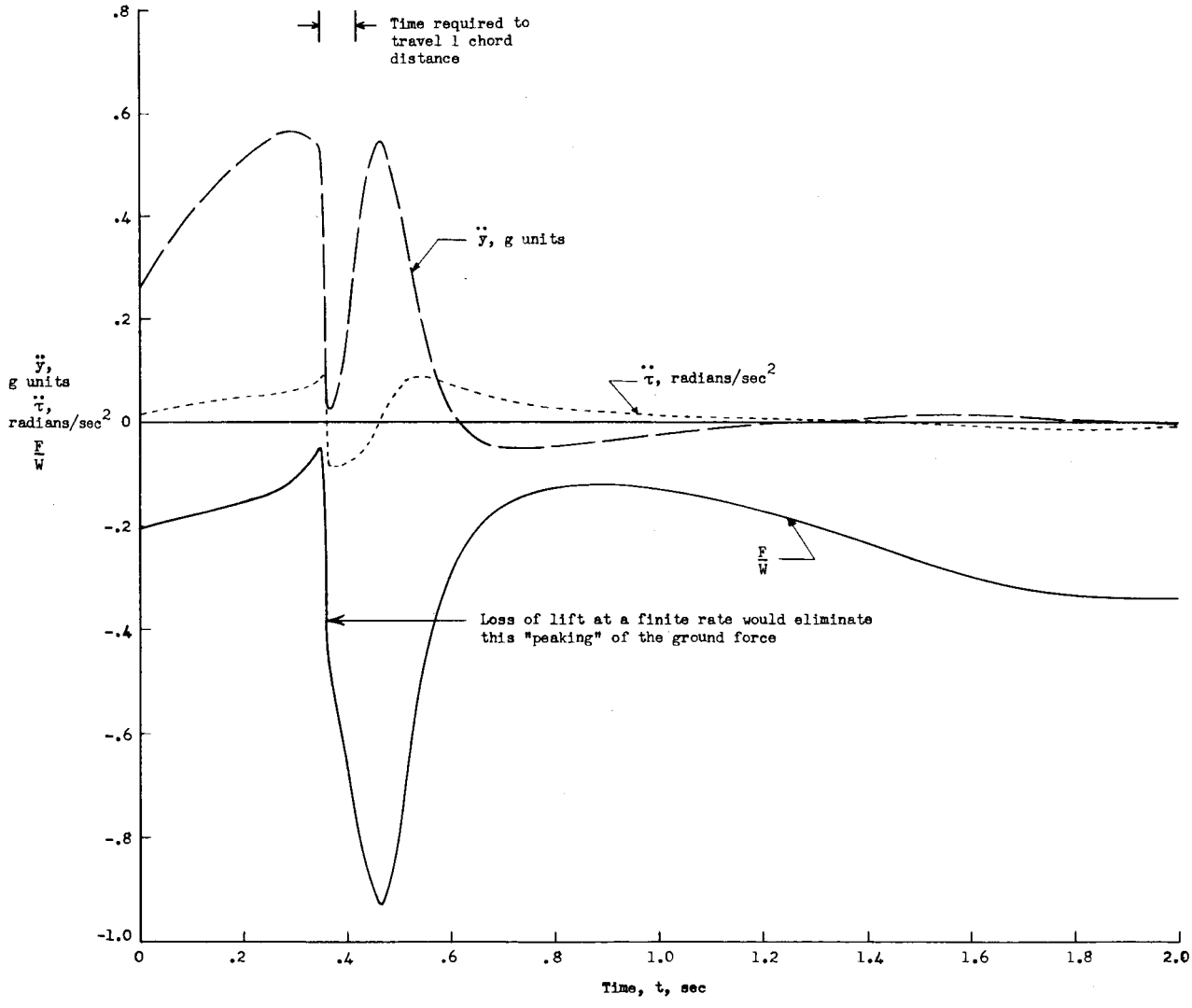

Figure 15.- Concluded.

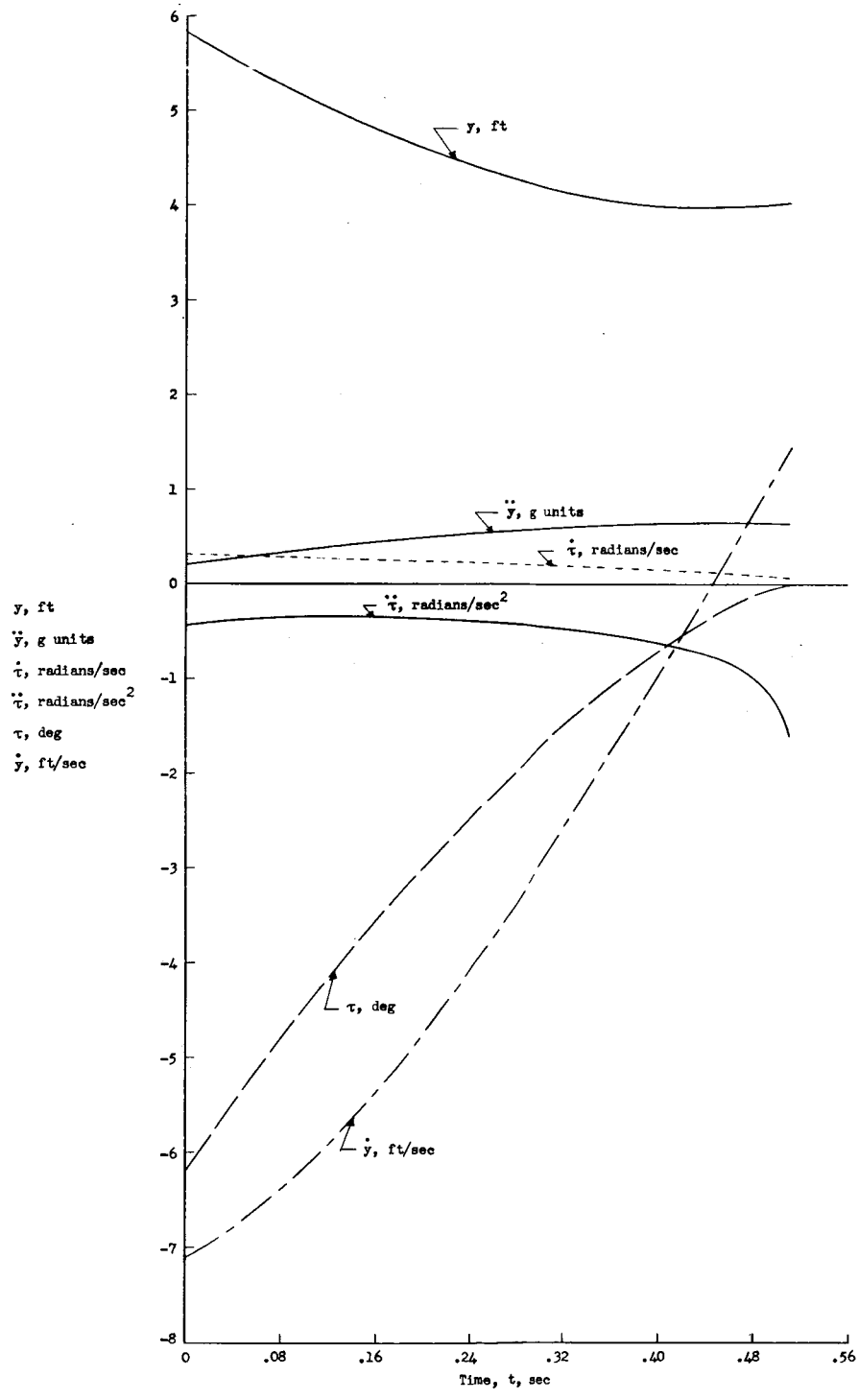

Figure 16.- Load and motion histories for nose-low landing. Modified contour.

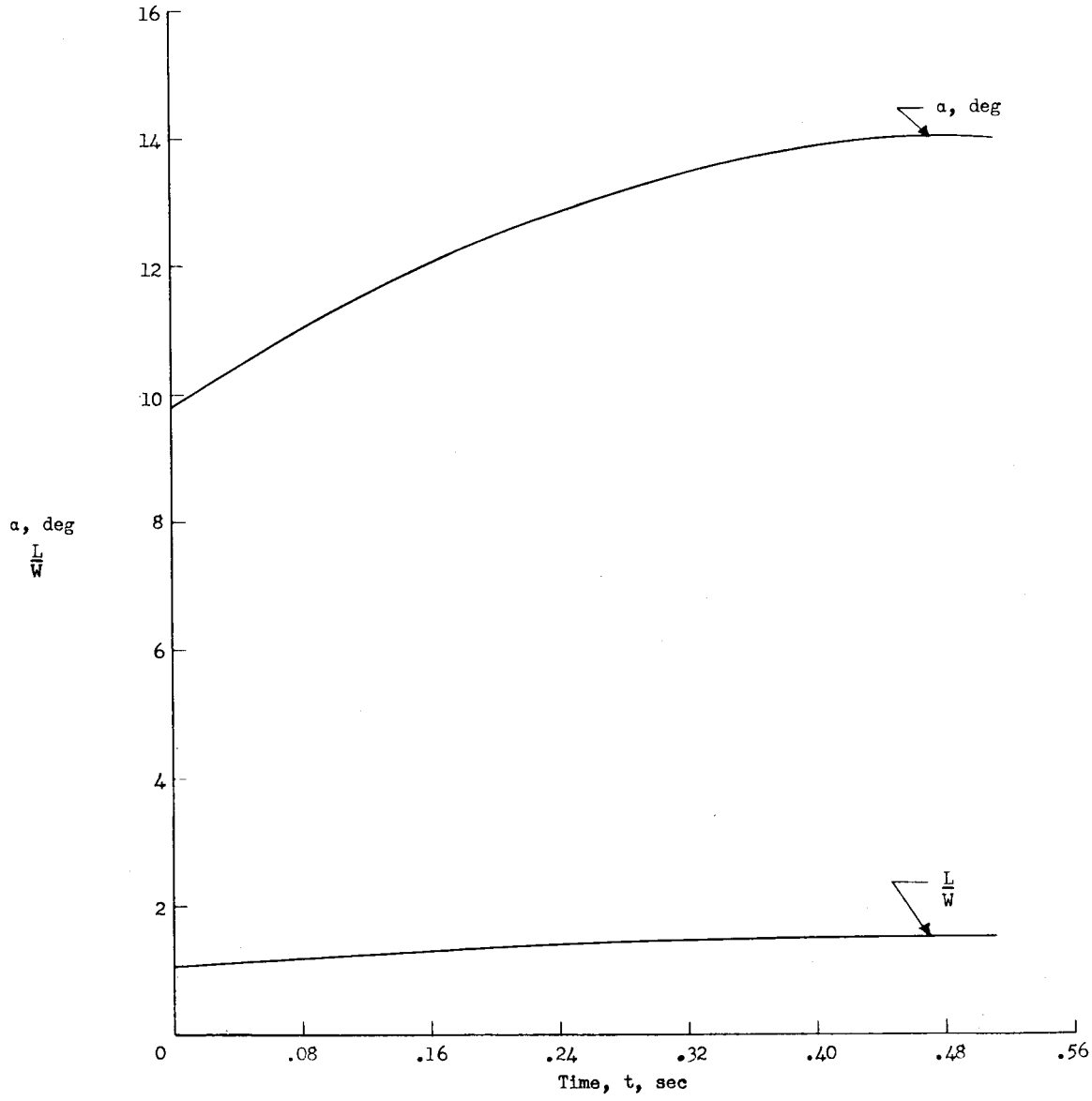

Figure 16.- Concluded.

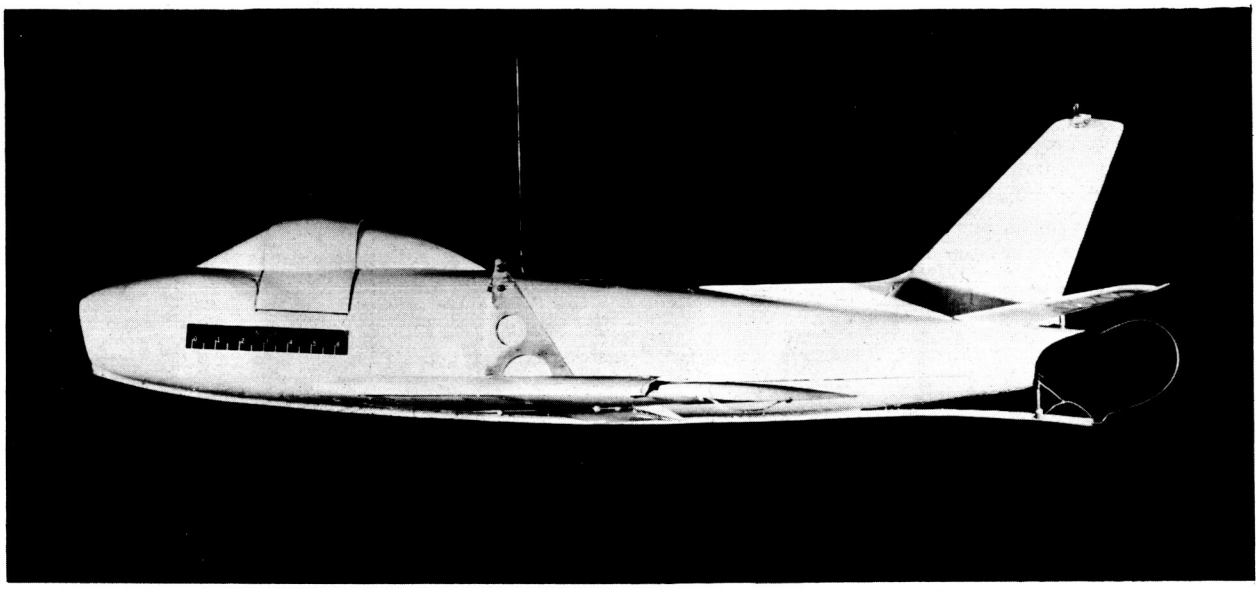

L-86292

Figure 17.- 1/10-scale dynamic model of a fighter with a rubbing strip fitted to the fuselage contour (case 13).

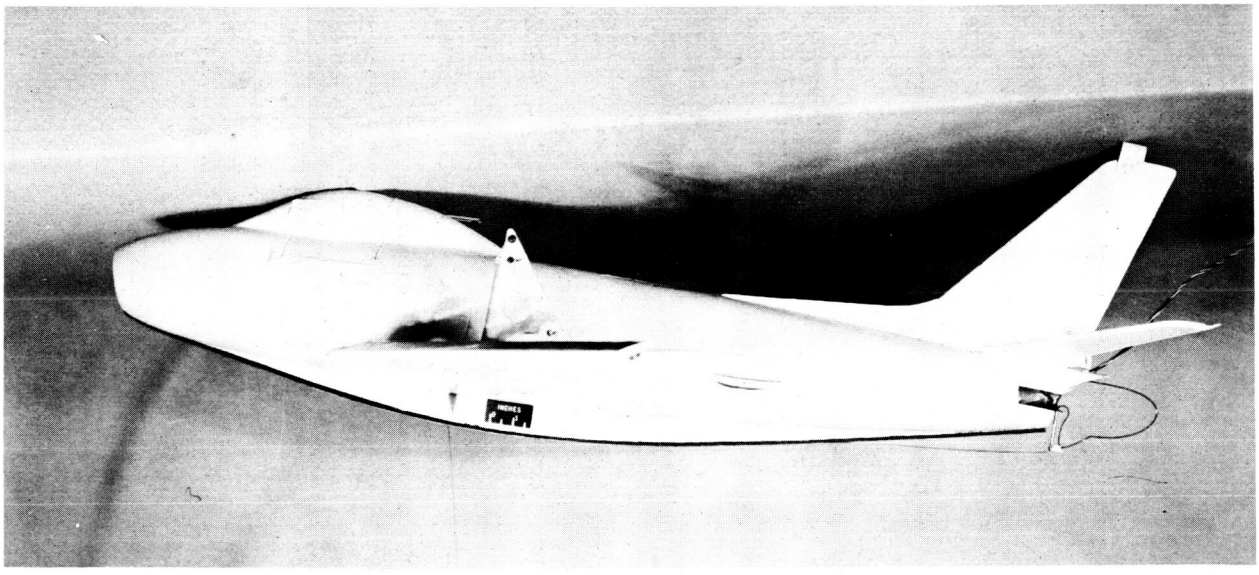

L-90408

Figure 18.- 1/10-scale dynamic model of a fighter with a computed rocker (case 14).

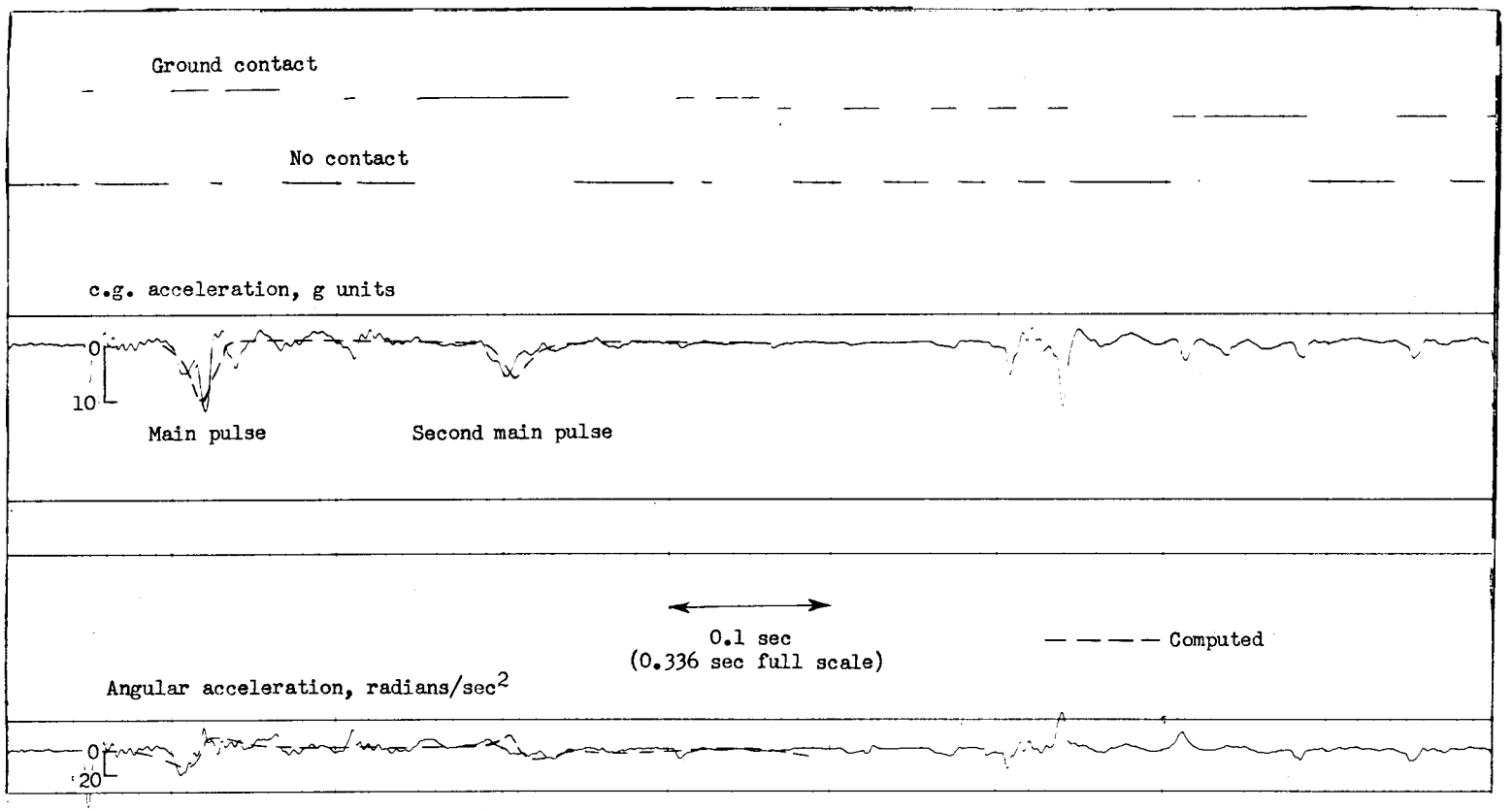

Figure 19.- Ground contact, vertical acceleration, and angular acceleration for landing of a model of a fighter on a rubbing strip fitted to the lower surface of the fuselage. Case 13 in table I.

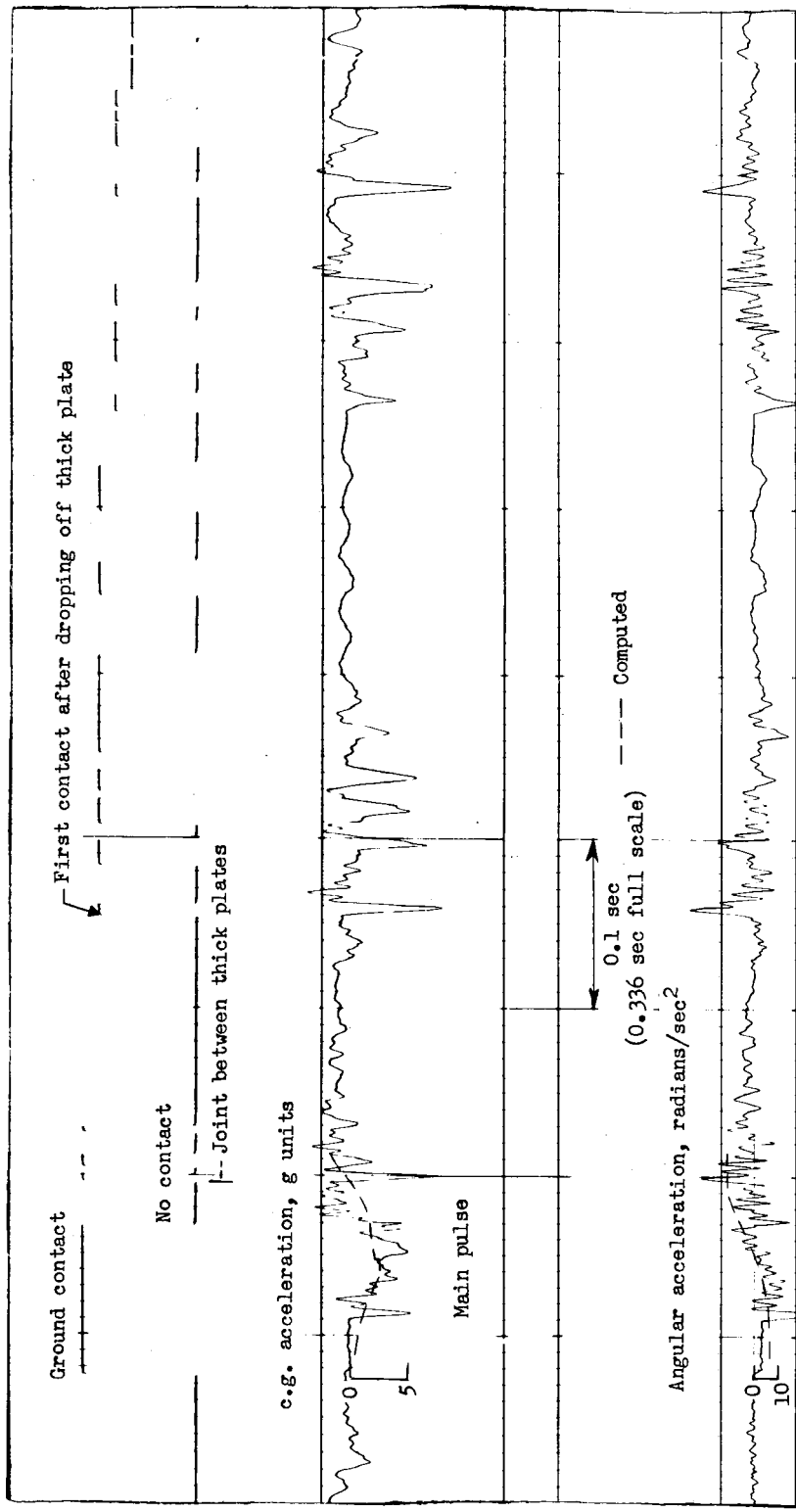

Figure 20.- Ground contact, vertical acceleration, and angular acceleration for landing of a model of a fighter on a computed rocker fitted to the lower surface of the fuselage. Case 14 in table I.

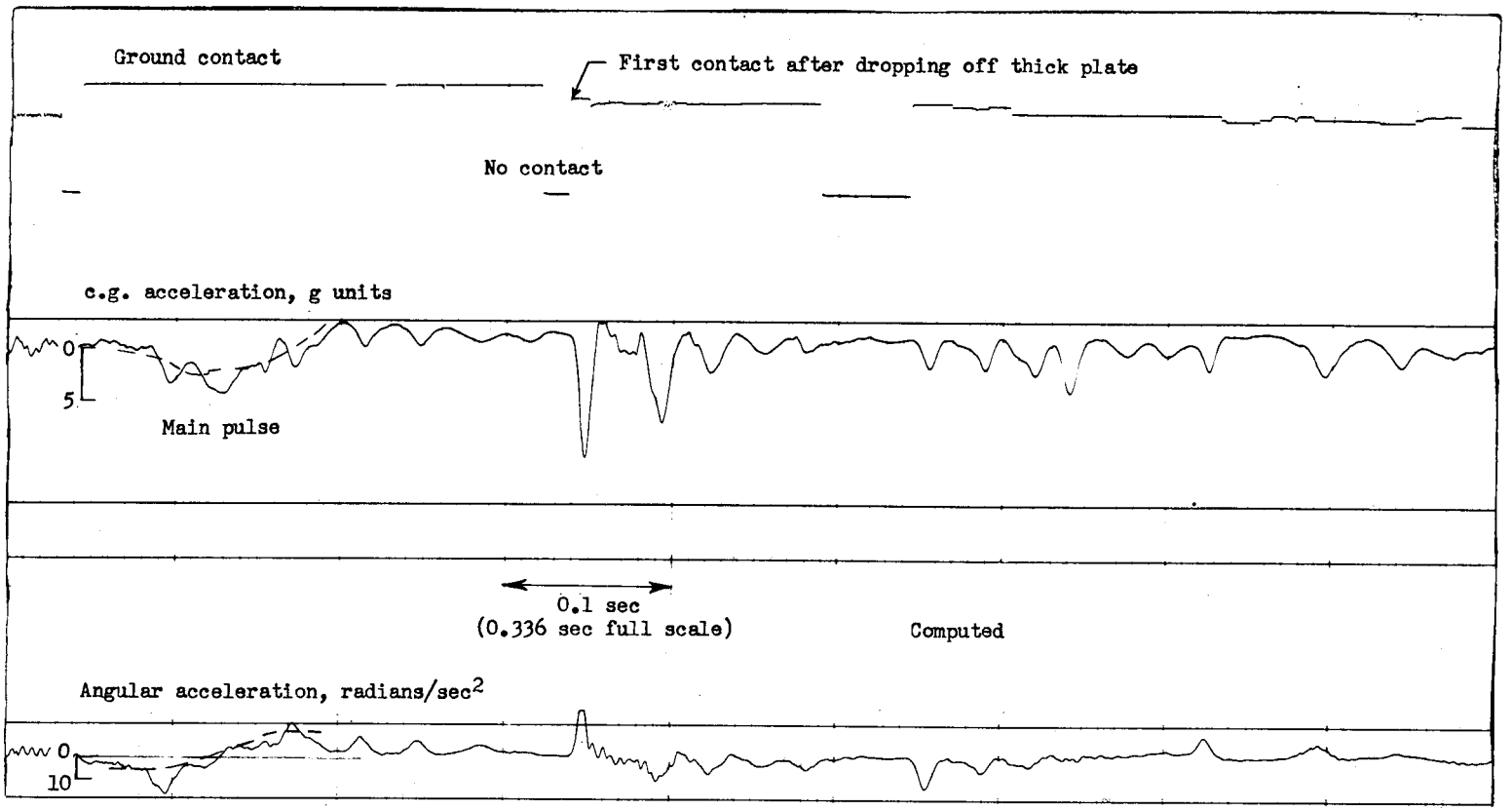

Figure 21.- Ground contact, vertical acceleration, and angular acceleration for landing of a model of a fighter on a computed rocker mounted on the lower surface of the fuselage with a rubber strip insert. Case 14 in table I.

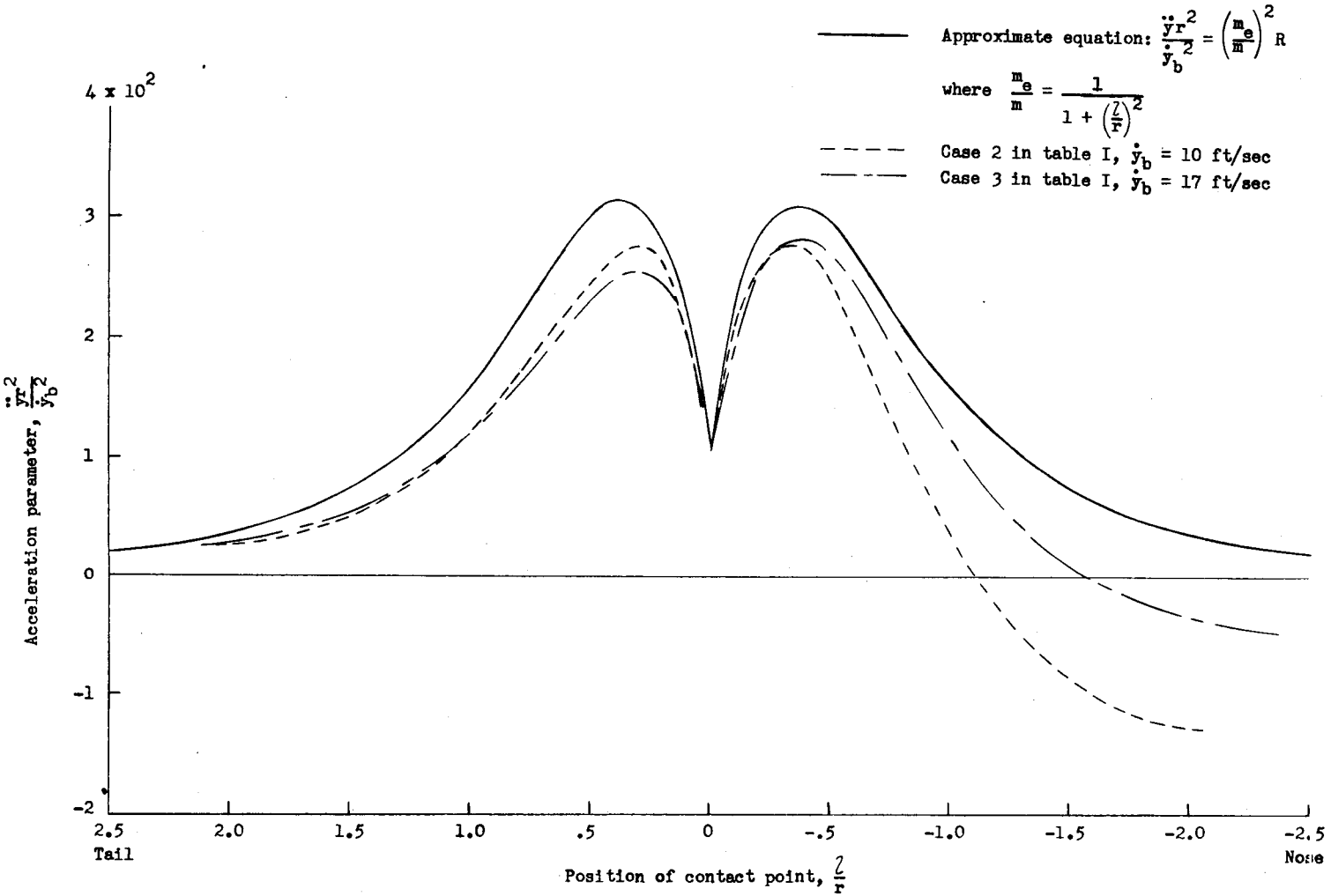

Figure 22.- Variation of acceleration parameter with position of contact point for an involute rocker.

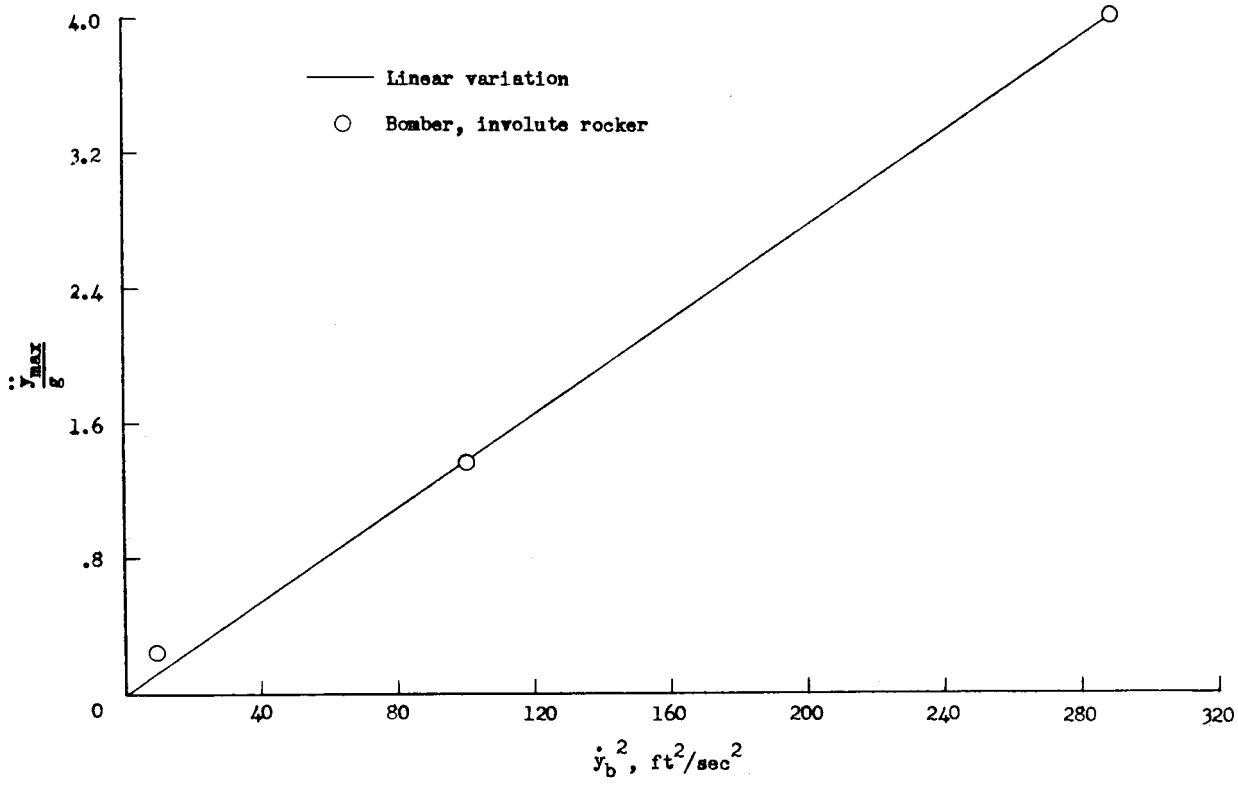

Figure 23.- Variation of vertical acceleration with sinking speed.

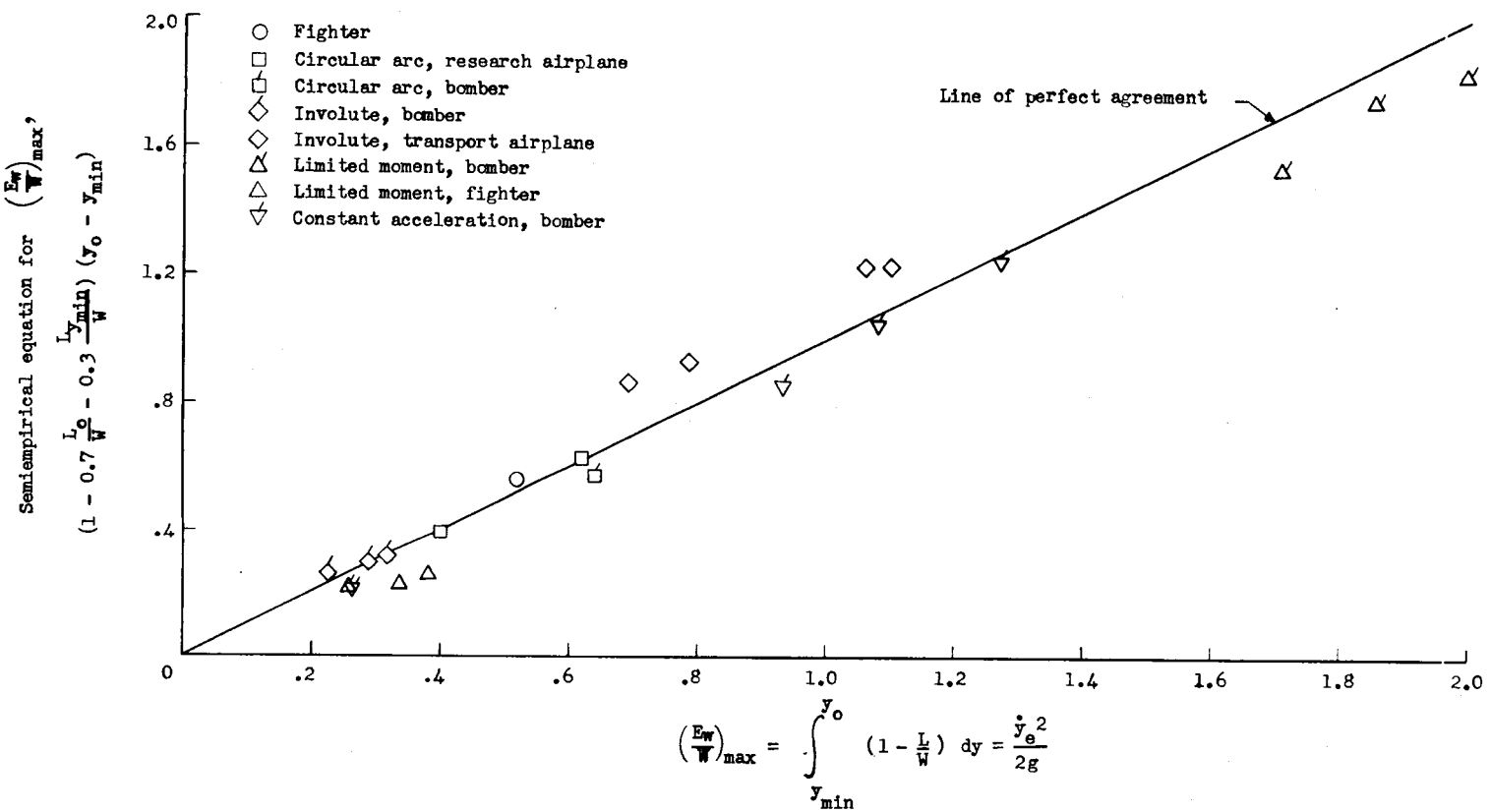

Figure 24.- Evaluation of approximate equation for the effect of unbalanced weight.

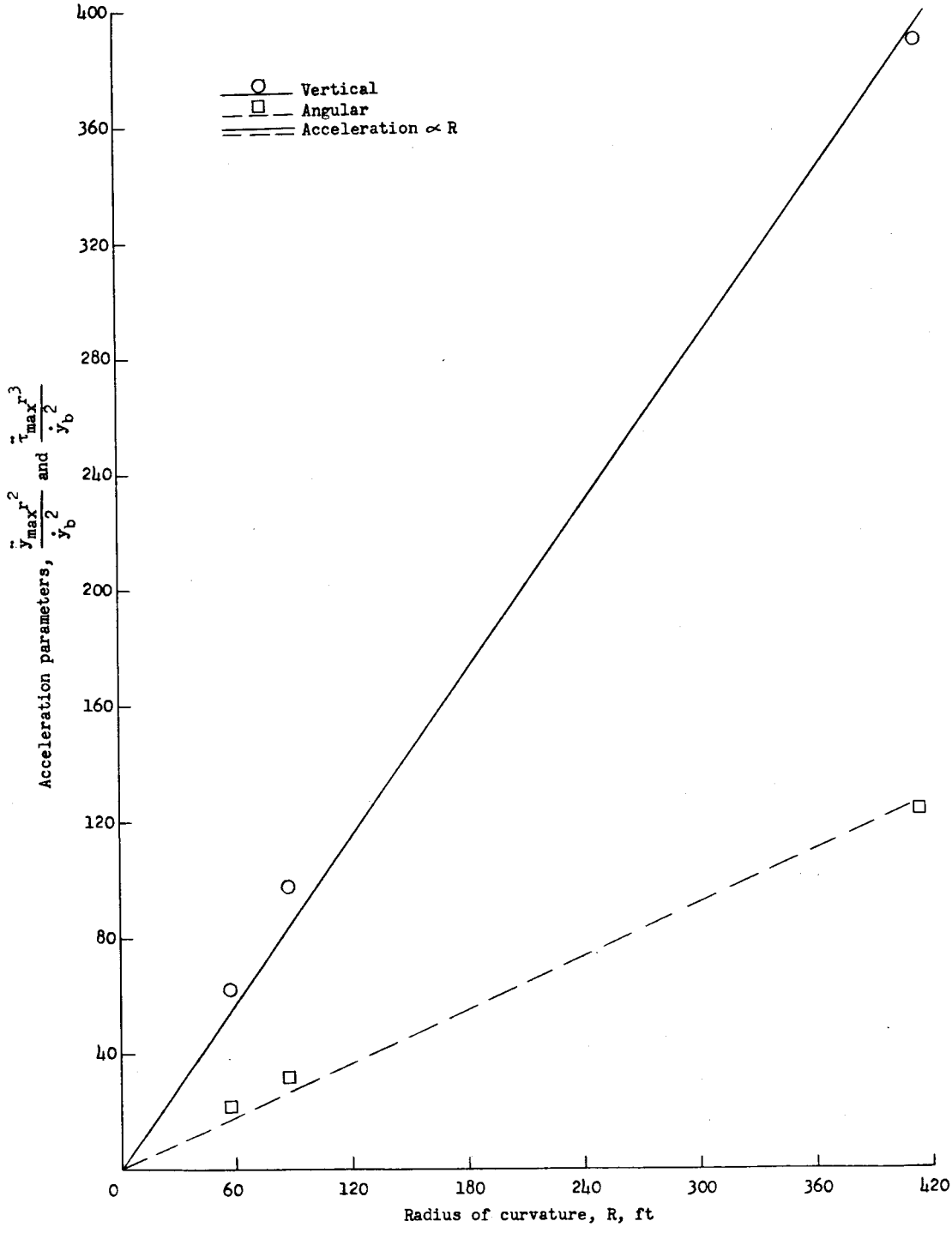

Figure 25.- Variation of acceleration parameters with radius of curvature.

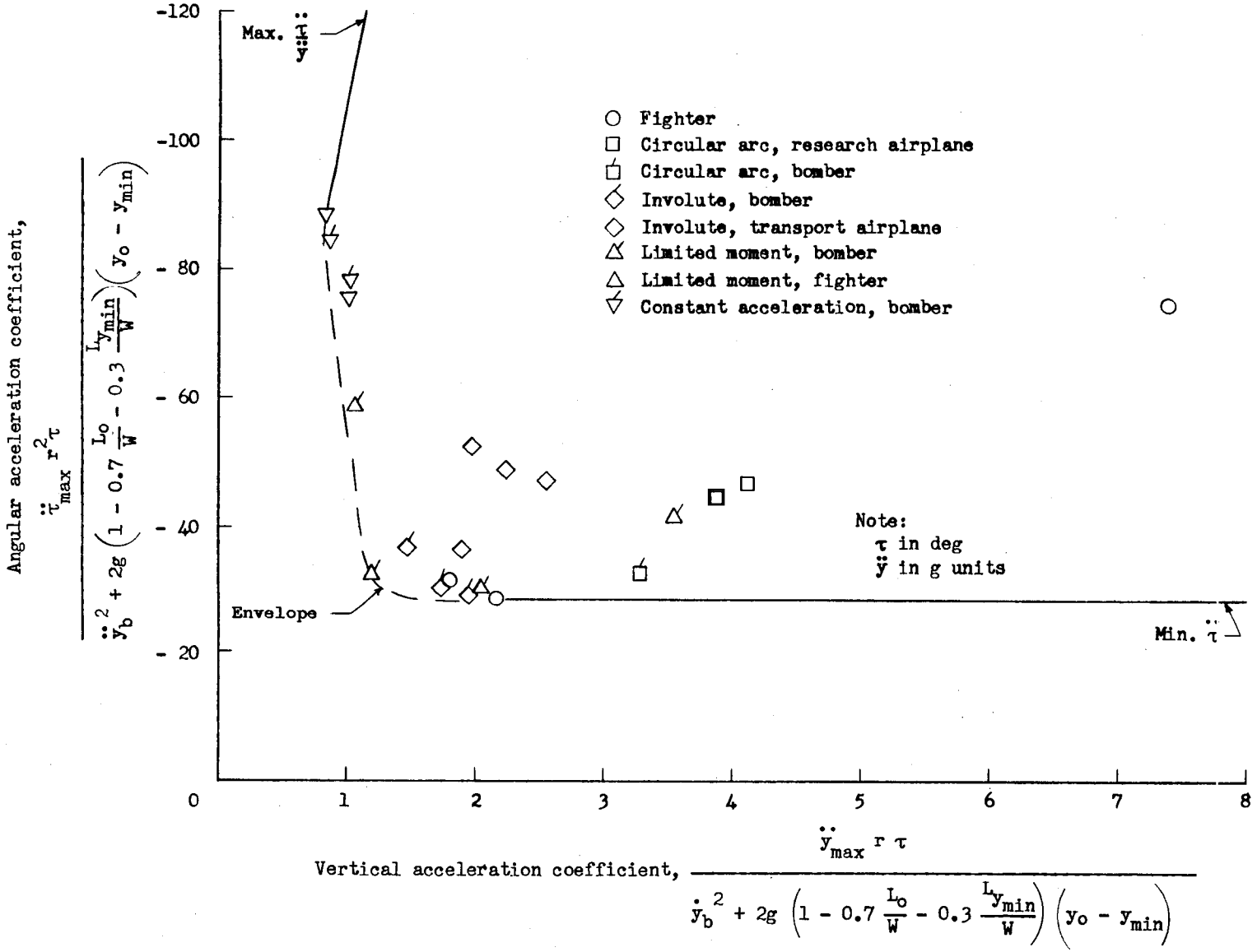

Figure 26.- Variation of maximum angular acceleration coefficient with maximum vertical acceleration coefficient.